12-11-2012

Theta Dynamics: Speed, Acceleration and Contribution to Cognition

Lauren L. Long
University of Connecticut - Storrs, lauren.long@uconn.edu

Theta Dynamics: Speed, Acceleration and Contribution to Cognition

Lauren Lynn Long

B.A., University of Connecticut, 2010

A Thesis

Submitted in Partial Fulfillment of the

Requirements for the Degree of

Master of Arts

at the

University of Connecticut

2012

APPROVAL PAGE

Master of Arts Thesis

Theta Dynamics: Speed, Acceleration and Contribution to Cognition

Presented by

Lauren Lynn Long, B.A.

Major Advisor _____

James J. Chrobak, Ph.D.

Associate Advisor _____

Monty A. Escabí, Ph.D.

Associate Advisor _____

Heather L. Read, Ph.D.

Associate Advisor _____

Chi-Ming Chen, Ph.D.

University of Connecticut

2012

Table of Contents

List of Figures

Chapter One: Introduction

Hippocampal Functionality

The hippocampal formation is an integral player in the creation of new memories. The neural and physical substrate of memory formation resides within the functional connectivity of ensembles of neurons and their dynamical interactions. Investigations into the function of ensemble activity, such as theta oscillations, has demonstrated its importance in relation to cognition, spatial navigation, path integration, and mnemonic functions in both humans (Kahana et al., 1999; Burgess et al., 2002; Fell et al., 2001; Sederberg et al., 2003; Ekstrom et al., 2005; Canolty et al., 2006; Knake et al., 2007) and non-human animals (Berry et al., 1978; Winson, 1978; Hasselmo et al., 2002; Wyble et al., 2004; Asaka et al., 2005; Buzsaki, 2005; Hasselmo, 2005; Kay, 2005; Jeewajee et al., 2008). While theta oscillations are thought to contribute to cognition, variation in the theta signal has been linked to locomotor indices and flow of sensory input impinging upon the hippocampal system.

Research regarding theta can be sub-divided into two interrelated categories: 1) those examining the underlying neural mechanisms that contribute to theta rhythm and frequency generation and 2) those attempting to link functional properties to characteristics of the ongoing rhythmic signal. Invariably, much research intertwines these distinct ideas. Early reports investigating the biological significance of theta oscillations noted its prominence during locomotion and the relationship between locomotor speed and the amplitude and

frequency of theta. (Vanderwolf, 1969; Teitelbaum & McFarland 1971; Feder & Ranck 1973; Whishaw & Vanderwolf, 1973; McFarland et al., 1975; Rivas et al., 1996). Based on differences in the frequency and behavioral correlates of theta oscillation, Bland and Oddie (2001) positied a key role for theta in sensorimotor integration. Mechanistically, the sensorimotor hypothesis states that type 2 theta (atropine sensitive and associated with immobility) is generated by medial septal cholinergic neurons. Functionally, these neurons serve to prime the motor system for activity. Then, if motor activity occurs, type 1 theta (atropine resistant and associated with locomotion) ensues in combination with motor output. Others suggest a continuum in underlying neural activity rather than two distinct theta types noting the dynamic involvement of medial septal GABAergic neurons, medial septal cholinergic neurons and the variety of subcortical afferents that determine the state of interactions between septal neurons in regulating theta (Lee et al., 1994). With this idea in mind, concerted network dynamics, such as theta oscillations may play a crucial role in sensorimotor interactions, initiating and engaging motor acts in order to integrate recent sensorimotor experience.

First we will briefly review the mechanisms that contribute to theta generation. Then, the current analyses of speed and acceleration will be discussed with regard to the function of the theta rhythm. In this regard, the presented analyses of speed and acceleration are part of an effort to characterize and quantify sources of variability in the amplitude and frequency of the theta signal. Further, we will describe how sources of variation differ across the septotemporal axis of the HPC. Lastly, we will discuss theta with regards to

sensorimotor processing, integration of sensory inputs, and ultimately how these indices contribute to cognition.

Hippocampal theta: the coordination of cell assemblies

The theta (6-12 Hz) rhythm can be observed in the local field potential (LFP) of the hippocampal formation (Green & Arduini, 1954; Petsche et al., 1962; Leung, 1985; Brankack et al., 1993; Bragin et al., 1995; Buzsaki, 2002). LFPs reflect the summation of extracellular currents that arise as a consequence of synchronized synaptic excitatory and inhibitory potentials impinging upon the highly laminar somatodendritic organization of hippocampal neurons. It is important to note that the principal neurons of the hippocampus (pyramids and granule cells) have an organized (laminar) arrangement of: 1) somatodendritic field and 2) afferent input terminating within that somatodendritic field (See Figure 1) and 3) intrinsic membrane oscillations of principal cells that resonate to inputs at theta frequencies (Green & Arduini, 1954; Petsche et al., 1962; Leung, 1984; Bland, 1986; Bragin et al., 1995; Vinogradova, 1995; Vertes & Kocsis, 1997; Buzsaki, 2002). Thus, for example, the apical dendrites of CA1 pyramidal neurons receive afferent input exclusively from layer 3 entorhinal cortical neurons within stratum lacunosum moleculare, while the afferent input from CA3 neurons onto CA1 neurons terminate within stratum radiatum (See Figure 1). Importantly, the highly organized architecture of the HPC allows for the summation of extracellular currents, ultimately leading to the observance of the rhythmic hippocampal field. LFP waveform characteristics, such as the frequency and

amplitude of the signal, depend on the proportional contribution of multiple afferent sources as well as intrinsic properties of brain tissue (Buzsaki et al., 2012). As a consequence, the LFP recorded throughout the HPC is drastically different in shape and amplitude depending on recording site (eg, CA1 vs DG).

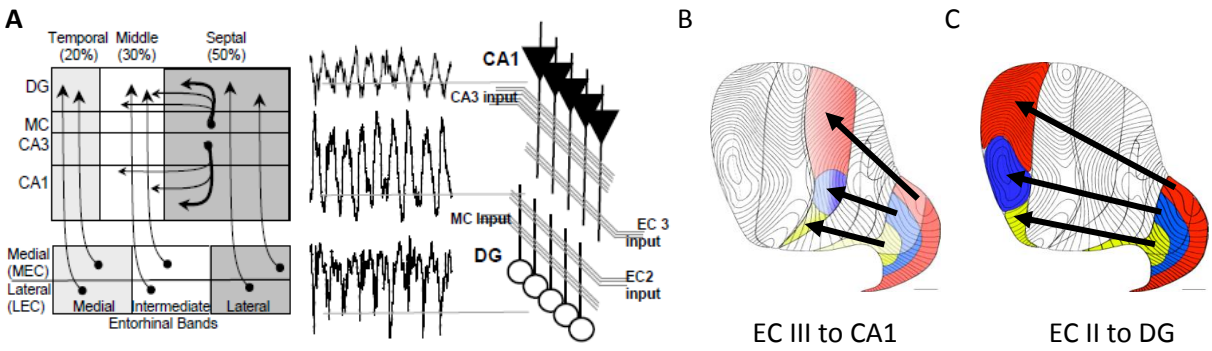

Figure 1. *Distinct EC bands project to distinct septotemporal extents*. **A**: Shows a more detailed schematic of synaptic contacts originating from EC, CA1 and mossy cells. The collaboration of excitatory inputs from CA3, ECIII to CA1, mossy cells and ECII to DG defines the extracellular theta LFPs in CA1 and the DG. **B**: Shows distinct EC bands that project to CA1. Outer band (lateral) is red, intermediate band is blue and inner (medial) band is yellow. The bands are orthogonal to cytoarchitectonic subdivisions of the EC (medial entorhinal area [MEA] and lateral entorhinal area [LEA]). The bands determine which areal or septotemporal level afferents terminate. **C**: Shows the same as B, but for DG.

Theta: current versus rhythm generation

As noted above, the LFP signal represents synchronized synaptic input within the laminarly organized somatodendritic field of HPC neurons. Mechanistically researchers have defined the currents that generate the time-varying LFP signal (current generation) as well as various sources that define the rhythmicity (rhythm generation). We will focus on rhythm and current generation with regards to CA1.

Rhythm generation represents the mechanisms that are responsible for the coordination of the synaptic potentials involved in current generation over time into a frequency limited phenomenon between 6-12 Hz**.** It's important to note that few of the key elements involved in theta current generation (EC, CA3, CA1 pyramids), fire faithfully at roughly 1-5 Hz in phase with theta rhythm (Buzsaki, 2002; Patel et al., 2012), while many GABAergic interneurons discharge at 40-100 Hz (Hajos et al., 2004; Ylinen et al., 1995) on each theta cycle. In addition to intrinsic properties of basket cells, the medial septum provides a divergent input to all major cells fields along the septotemporal axis, including the EC.

To provide "rhythm" to the theta oscillation, the medial septum serves as a pacemaker to regulate the frequency of the theta oscillation. Neurons important for this massive coordination of theta field potentials are medial septal cholinergic neurons (Brazhnik & Fox, 1999), medial septal GABAergic neurons that selectively target specific sub-populations of hippocampal GABAergic neurons

(Freund & Antal, 1988; Borhegyi et al., 2004), medial septal glutamatergic projections (Colom et al., 2005), and hippocampo-septal neurons that selectively target medial septal GABAergic neurons (Toth et al., 1993; Manseau et al., 2008). While the medial septum appears to play the most important role in theta rhythm generation, subcortical inputs have the potential to participate in generating theta rhythmicity as well as modulating ongoing interactions among elements of the hippocampal circuit. Notably, serotonergic input originating from the locus coeruleus, noradrenergic projections from the raphe nucleus and histaminergic input from the tuberomamillary nucleus of the posterior hypothalamus (Vertes & Kocsis, 1997; Fano et al., 2011) all impinge upon the hippocampus. The joint participation of the highly topographic input of medial septal and subcortical afferents allows for the observance of the highly regular hippocampal theta rhythm.

While rhythm generation refers to the mechanisms that are responsible for the coordination of the synaptic potentials, *current* generation refers to the synaptic potentials that generate the extracellular currents that are recorded as the local field potential and lead to the rhythmic field oscillation. Several key players contribute to theta current generation in CA1 of the HPC. First, rhythmic afferent excitation from EC layer III neurons impinge upon the distal dendrites of CA1 cells (Alonso and Garcia-Austt, 1987; Chrobak and Buzsaki, 1998). Without this prime input from the EC, theta field oscillations are diminished (Bragin et al., 1995). Furthermore, intrinsic excitatory hippocampal neurons arising from CA3 pyramidal (principal) neurons contribute to theta generation (Kocsis & Buzsaki,

1999; Buzsaki, 2002). Moreover, local GABAergic interneurons (soma and dendritic targeting; Konopacki et al., 1992; Ylinen et al., 1995; Hajos et al., 2004) provide for the current generation of theta oscillations.

Areal & laminar organization of the HF: functional differentiation

As stated earlier, several key players contribute to theta generation in CA1 of the HPC. Rhythmic afferent excitation from EC layer III neurons impinge upon the distal dendrites of CA1 cells (Alonso and Garcia-Austt, 1987; Chrobak and Buzsaki, 1998). Moreover, intrinsic excitatory and inhibitory neurons arising from CA1 also participate in the generation of the theta rhythm (Ylinen et al., 1995; Konopacki et al., 1992; Hajos et al., 2004). First, the primary focus will concern variation in the theta signal across the septotemporal axis of CA1 with regards to theta current generators, as stated above. Then, septotemporal variation in subcortical inputs and how such variation contributes to septotemporal dynamics of the theta signal.

Similar to the neocortex, which receives inputs from topographically distinct neocortical and thalamic areas; the septotemporal axis of the hippocampus is analogous to an areal region of neocortex and receives inputs from distinct regions of the EC, that in turn receive inputs from associative cortices (Dolorfo & Amaral, 1998a; Burwell, 2000; Lavenex & Amaral, 2000; Chrobak & Amaral, 2007). The EC can be segregated into distinct mediolaterally

oriented bands (outer, intermediate and inner) that project to different septotemporal extents of the HPC (Dolorfo & Amaral, 1998a)**.** The septal half of the hippocampus receives input from the outer (lateral) band of the EC, mid-septotemporal (next ~ 25%) hippocampus receives projections from the intermediate band of the EC and the inner (medial) band of the EC projects to temporal hippocampus (last ~25%) [Fig.1B & 1C]. These EC bands are orthogonal to cytoarchitectonic subdivsions of the medial and lateral entorhinal areas (Dolorfo & Amaral, 1998a; Burwell, 2000; Lavenex & Amaral, 2000; Chrobak & Amaral, 2007). With regard to laminar organization, EC layer II stellate cells terminate on the dendrites of DG molecular layer granule cells and on the distal apical dendrites of pyramidal cells in stratum lacumosum-moleculare (SLM) of CA3 (perforant path) [See Figure 1]. EC layer III pyramidal cells project to the distal apical tufts of pyramidal cells in SLM of CA1 and the molecular layer of the subiculum (temporoammonic path). These afferents provide the primary neocortical input to the HPC and thus participate in the well described DG>CA3>CA1 trisynaptic loop. The output of CA1 and the subiculum conveys hippocampal processing back to the EC. Thus, the EC is the primary recipient of hippocampal output, which terminates in its deep layers (V & VI). More specifically, pyramidal cells of CA1 and the subiculum send return projections to layers V and VI of the EC (Fig. 1A). While the layer of origin in the EC (eg, II-III) determines the organization of sub-regional termination within the transverse axis of the hippocampus, it is important to make clear that the areal organization of the EC (bands) determine afferent termination across the areal axis of the HPC

(septotemporal or longitudinal axis). As stated earlier, EC afferents are a major theta current generator, and as depicted in Figure 1, segregate groups of cells project to distinct septotemporal extents. This characterization suggests that the EC may be a potential source of amplitude differences observed in theta across the septotemporal axis.

In addition to EC afferents, all hippocampal cell fields receive a unique complement of intrinsic inputs. Evidence suggests that distinct network states (eg, theta, sharp waves) can be defined by variation in the strength of instrinsic versus extrinsic inputs impinging on CA1. Prominent intrinsic connections include mossy cells originating from the hilus of the DG that make synaptic contact onto DG granule cells (Amaral & Witter, 1989). These granule cells, more specifically their mossy fiber axons, send reciprocal projections back onto mossy cells, thus creating a recurrent loop of synaptic contact. Additionally, mossy fibers of granule cells project in a unidirectional manner to principal cells of CA3 (Henze et al, 2000). CA3 pyramids have recurrent collateral connections, synapsing upon themselves, thus creating a continual loop of synaptic contact (Henze et al., 2000). The Schaffer collaterals (axons) of CA3 principal cells project to CA1 principal cells, while CA1 cells project to subicular pyramidal cells. With these ideas in mind, theta LFPs are dominated by two distinct sets of excitatory inputs. CA1 neurons receive CA3 Schaffer collateral afferents as well as input from EC layer III, while granule cells receive input from mossy cells and EC layer II neurons (Amaral & Witter, 1989). Changes in theta coherence across the septotemporal axis could reflect a shifting dynamic between these two sets of

excitatory inputs on CA1 and DG. Slight alterations in the frequency of theta, and thus the timing of inputs could bias CA1 neurons to listen to either CA3 or EC input (Ang et al., 2005; Sabolek et al., 2009 discussion). Furthermore, it is important to note that while segregate EC bands that project to distinct septotemporal regions could produce observed differences in the LFP pattern, mossy cells project extensively across the septotemporal axis and in this manner, could provide a means for synchronizing the theta signal, while differential EC inputs could serve to "segregate" the theta signal.

Subcortical projections to the hippocampal formation

Medial septum & diagonal band of Broca

Another source of theta variability along the septotemporal axis arises from septohippocampal input. The medial septum (MS) sends topographically arranged cholinergic and GABAergic projections across the septotemporal axis. More specifically, neurons located anteriorally and laterally in the MS project to temporal HPC, while cells located posteriorally and medially project to septal HPC (Mosko et al., 1973; Nyakas et al., 1987; Gaykema et al., 1990). Because the medially situated neurons in the medial septal nucleus tend to be GABAergic rather than cholinergic, septal levels of the DG receive most cholinergic input from the nucleus of the diagonal band. In contrast, temporal levels of the DG receive cholinergic innervation primarily from the medial septal nucleus (Baisden et al., 1984; Amaral & Kurz, 1985; Wainer et al., 1985; Lubke et al., 1997). The

MS projections terminate most heavily in stratum oriens of CA1, with CA3 receiving substantially less input from the MS. In the DG, MS cells terminate most heavily in the polymorphic layer (Mosko et al., 1973; Nyakas et al., 1987). Moreover, MS GABAergic neurons target hippocampal GABAergic basket cells. Since MS GABAergic cells spike in phase with theta (King et al., 1998; Brazhnik & Fox, 1997; 1999), this septohippocampal GABAergic projection provides theta rhythmic inhibition to hippocampal basket cells, which allows these cells to powerfully control the spike rate of hippocampal principal cells (Freund & Antal, 1988). In contrast, septohippocampal cholinergic projections terminate more diffusely and contact excitatory and inhibitory cells (Baisden et al., 1984; Amaral & Kurz, 1985; Wainer et al., 1985). These cholinergic cells provide an overall depolarizing effect to all hippocampal cells (Bernardo & Prince, 1982; Pitler & Alger, 1992). While cholinergic medial septal cells are thought to contribute to alternations in theta amplitude changes (Lee et al., 1994; Buzsaki, 2002), they lack the temporal resolution to contribute to rapid changes in theta power (Zhang et al., 2010), whereas cells that participate in theta current generation have the ability to produce theta amplitude changes on a finer temporal scale. Further, with segregate MS neurons projecting to differential septotemporal extents of the HPC, the MS is well suited for synchronizing or desynchronizing the theta rhythm across the longitudinal axis.

Other subcortical projections to the hippocampal formation

The major excitatory hypothalamic input to the HPC arises from the supramammillary and tuberomammillary nuclei (Kiss et al., 2000). This nucleus preferentially targets the DG with few projections in CA1 (Vertes, 1992). The supramammillary projections show a graded distribution across the longitudinal axis with a denser termination in septal HPC than in temporal HPC (Vertes, 1992). These neurons fire at theta frequency (Kocsis & Vertes, 1994; Pan & McNaughton, 1997; Kirk, 1998) and in addition to targeting the HPC, these neurons target MS neurons, providing a depolarizing effect that could increase the rhythmicity of MS neurons (McNaughton et al., 1995; Kirk et al., 1996; Borhegyi et al., 1997). Second, the nucleus reuniens is the sole source of thalamic input to the hippocampal formation (Herkenham, 1978; Wouterlood et al., 1990; Dolleman-Van der Weel & Witter, 2000). The nucleus reuniens, located on the midline, gives rise to a prominent projection to SLM of CA1 to both principal and GABAergic interneurons, where it overlaps with EC fibers. Furthermore, this nucleus innervates all septotemporal levels of CA1 with a preference for mid-septotemporal levels (Dolleman-Van der Weel & Witter, 2000). Thirdly, tracing methods demonstrate that temporal CA3 receives input from the amygdaloid complex, which was previously thought to only send projections to CA1 and the subiculum (Pikkarainen et al., 1999; Pitkanen et al., 2000). These substantial distinctions in subcortical input along the septotemporal axis not only create differences in the measured LFP signal, but serve to functionally differentiate the septotemporal axis.

Distribution of neuromodulatory inputs to the hippocampal formation

The DG receives a prominent noradrenergic input arising from the locus coeruleus (LC). These fibers terminate mostly in the polymorphic layer of the DG as well as in SLM of CA3 and CA1 (Pickel et al., 1974; Swanson & Hartman, 1975; Loughlin et al., 1986). However, LC innervation is similar at all septotemporal extents (Loy et al., 1980). Like noradrenergic input, serotonergic input from the raphe nucleus (RN) terminates most heavily in the polymorphic layer of the DG and SLM of CA1 (Conrad et al., 1974; Moore & Halaris 1975; Kohler & Steinbusch, 1982; Vertes et al., 1999). A large number of GABAergic interneurons appear to be preferentially innervated by serotonergic afferents (Halasy et al., 1992; McMahon & Kauer, 1997). Thus, the few serotonergic fibers innervating the HPC could have a crucial action by enhancing GABAergic inhibitory activity of hippocampal interneurons. Moreover, serotonergic innervation increases from septal to temporal levels (Oleskevich & Descarries, 1990). Lastly, histaminergic input from the tuberomamillary nucleus of the posterior hypothalamus (Vertes & Kocsis, 1997; Fano et al., 2011) increase from septal to temporal levels (Panula et al., 1989; Loy et al., 1980; Haring & Davis, 1985; Bjarkam et al., 2003; Gage & Thompson, 1980; Amaral and Kurz, 1985; see also Thompson et al, 2008 for review).

Physiological functional differentiation across the longitudinal axis

Historically, significant emphasis has been placed on examining the functionality of distinct hippocampal subregions within the trisynaptic circuit (DG > CA3 > CA1) of septal hippocampal regions rather than functional differences across the areal or longitudinal expanse of the HPC (Anderson et al., 1971). Markedly, physiological findings in septal HPC have been attributed to the entirety of the septotemporal axis, suggesting that the HPC acts as a unitary structure for successful information processing. A variety of behavioral studies based largely on lesion data in rodents and neuroimaging data in humans support functional differentiation of hippocampal circuits along the long axis (Moser et al., 1995; Strange et al., 1999; see Bannerman et al., 2004 for review). Additionally, there is considerable septotemporal variation in neuronal markers (Gusev et al., 2005), neuromodulation of plasticity (Maggio & Segal, 2007), and differences in the experiences that influence neurogenesis along the long axis (Snyder et al., 2009). While LFP data support functional differentiation across the longitudinal axis, the work of place cells provides convincing evidence that suggests variability in the spatial representation written across the surface of the septotemporal axis.

Principal cells in septal CA1 have long been demonstrated to have spatially restricted receptive fields, or “place fields” in a given environment (O’Keefe & Dostrovsky, 1971). These septal CA1 “place cells” are believed to provide a cognitive spatial representation of a given environment, with as few as

15-20 place cells predicting a rat's location in space within a few centimeters (Wilson & McNaughton, 1993). The vast majority of place cell work has strictly focused on the well-defined place fields of septal CA1 (Jung et al., 1994; Maurer et al., 2005; Kjelstrup et al., 2008; Lubenov & Siapas, 2009; Royer et al., 2010), while the few studies which have recorded from place cells at temporal extents have demonstrated that place field size systematically increases across the septotemporal axis (Jung et al., 1994). Place fields in septal HPC are small, concise, and refined, while in temporal HPC, place field sizes become much larger, reaching at least a meter in length (Jung et al., 1994; Maurer et al., 2005). Furthermore, recordings in CA3 principal cells across the septotemporal axis show place fields 5-6 meters in length when rats traverse an eighteen meter long linear track (Kjelstrup et al., 2008). Royer el al., 2010 confirmed the increase in place field size in CA3 temporal HPC and suggested that non-spatial information was also coded by temporal CA3 principal cells. More specifically, CA3 principal cells dissociate between open versus closed arms on a radial maze as well as traversals toward and away from a reward positioned at the end of the arm (Royer et al., 2010). These data taken together suggest functional differentiation across the septotemporal axis of the HPC, further indicating that perhaps septal cells code for interoceptive (egocentric) information, while temporal cells code exteroceptive (allocentric) information.

The effect of locomotor indices on theta amplitude

In addition to anatomical variation and the differences in place cell physiology, recent work supports variation in LFP signals across the septotemporal axis of the HPC (Maurer et al., 2005; Sabolek et al., 2009; Hinman et al., 2011; Penley et al., 2011; Patel et al., 2012). Early work investigating the behavioral correlates of the hippocampal theta signal observed its emergence during locomotion, specifically running speed of the rodent (Vanderwolf, 1969; Teitelbaum & McFarland, 1971; Whishaw and Vanderwolf, 1973; Feder & Ranck, 1973; McFarland et al., 1975). Furthermore, it has been shown that in septal HPC not only theta power, but theta frequency increases as a function of running speed (Rivas et al., 1996; Slawinska & Kasicki, 1998; Shin & Talnov, 2001). The increase in theta power as a function of running speed has been established in more recent studies examining the septal pole of the HPC (Rivas et al., 1996; Bouwman et al., 2005) as well as functional differentiation of the theta signal across the longitudinal axis of the HPC (Hinman et al., 2011). Maurer and colleagues suggested that the positive linear association between theta amplitude and running speed decreases at mid-septotemporal levels, but lack of simultaneous recordings made it impossible to validate such a suggestion. Hinman et al., 2011, addressed the suggestion of Maurer et al. (2005) demonstrating that the positive linear association between speed and theta power systematically decreases with distance from the septal pole. This work further supports functional differentiation across the septotemporal axis.

Goals of current research

Our laboratory is predominantly interested in defining sources of variability in the theta signal as it relates to online sensorimotor processes. In this regard, hypotheses regarding the biological significance of theta oscillations suggest its role in learning and memory encoding/consolidation. With this idea in mind, typically rodents locomote through an environment in which learning and memory operations are present (Montgomery et al., 2009). Given the knowledge that much variability in the theta signal can be attributed to locomotion, it is essential to control for movement related indices in order to parse out the relative contribution of the theta signal to learning and memory processes. In this vein, Vanderwolf (1971) has highlighted the necessity for sufficient control of movement in experimental designs linking altered theta oscillations to mnemonic and cognitive operations, while other studies have deemphasized the contribution of locomotor indices (Montgomery et al., 2009). A better understanding of the relative contribution of these highly quantifiable variables and their potential dynamic variation should facilitate analyses of how alterations in theta indices relate to cognitive/memory processes. Besides speed of the animal, little to no work has examined the role of other locomotor indices, such as whole body acceleration of the animal and its relation to theta indices, or how this relationship varies across the septotemporal axis of the HPC, although investigators discuss the possible contribution of acceleration in modulating theta indices (Whishaw, 1972; Arnolds et al., 1984; Wyble et al., 2004; Bland et al., 2006). With these ideas in mind, our laboratory is particularly interested in

defining sources of variability in theta indices across the septotemporal axis of the HPC, with the general hypothesis that theta indices will be constrained under distinct sensory of behavioral conditions.

The current study investigated the contribution of acceleration to theta amplitude across the longitudinal axis of CA1 and DG, in attempt to further define sources of variability in theta indices. We show that whole body acceleration of the animal is a significant predictor of theta amplitude at septal hippocampal sites, over and above the influence of locomotor speed and that deceleration is more predictive of theta amplitude than acceleration. Furthermore, the relationship between deceleration and theta amplitude decreases as a function of distance from the septal pole in CA1 but not in DG, while the influence of acceleration remains constant across the septotemporal axis.

Chapter Two: Manuscript

Abstract

Theta (6-12 Hz) rhythmicity in the local field potential (LFP) and neuronal discharge reflect a clocking mechanism that brings physically isolated neurons together in time, allowing for the integration and segregation of distributed cell assemblies. Variation in the theta signal has been linked to locomotor speed, sensorimotor integration as well as cognitive processing. Mechanistically, variation in the LFP signal results from variation in the synaptic input impinging upon neuronal elements as well as intrinsic membrane oscillations consequent to synaptic input. Previously, we have characterized the relationship between locomotor speed and theta power and how that relationship varies across the septotemporal (long) axis of the hippocampus. The current study investigated the relationship between acceleration (positive acceleration) and deceleration (negative acceleration) and theta indices at CA1 and dentate gyrus (DG) sites along the septotemporal axis of the HPC. Our findings demonstrate that acceleration and deceleration predict a significant amount of the variability in the theta signal. We also demonstrate that deceleration is more predictive of variation in theta amplitude as compared to acceleration as rats traverse a linear track. Further, while the relationship between deceleration and theta power decreased across the long axis, most notably in region CA1, the relationship of acceleration to theta power did not vary across the long axis. Such findings highlight key variables that can be systematically related to dynamics in the theta

signal as it varies across the long axis of the hippocampus. A better understanding of the relative contribution of these quantifiable variables and their dynamic variation should facilitate our understanding of laminar and septotemporal variation in the theta signal as well their potential relation to sensorimotor and/or cognitive processes.

Introduction

The laminar organization of the HPC provides an optimal architecture for the generation of large amplitude local field potentials (LFPs) such as theta or sharp waves (Buzsaki, 1989; Chrobak & Buzsaki, 1994; Lee et al., 1994; Buzsaki, 2002). These LFP signals reflect the summation of local excitatory and inhibitory synaptic potentials impinging upon the somatodendtric field of hippocampal neurons. The theta signal in particular reflects rhythmic (6-12 Hz) inputs that facilitate temporal interaction among the relatively autonomous neurons, allowing for the integration and segregation of distributed cell assemblies (eg, Llinas et al., 1991; Gray, 1994; Bragin et al., 1995; Buzsaki & Chrobak, 1995; Lisman & Idiart, 1995; Buzsaki, 2002; Harris et al., 2003; Lisman, 2005; Dragoi & Buzsaki 2006).

The theta signal has been linked to cognitive variables across several mammalian species (eg, Ulanovsky & Moss, 2007; Montgomery et al. 2009) as variation in the signal can correlate directly with the strength of encoding as evidenced by a relation to subsequent memory performance (Rizzuto et al., 2006; Sederberg et al., 2003; see Jutras & Buffalo, 2010 or Nyhus & Curran 2010 for reviews). Historically, moment-by-moment variation in the amplitude and frequency of theta in the rodent HPC has been associated with locomotor speed and linked to sensorimotor/path integration (see Bland and Oddie, 2001; Wyble et al., 2004; Sinnamon, 2006 for reviews). Recent findings have highlighted significant variation in the amplitude and coherence of the theta signal across its septotermporal areal or long axis (Sabolek et al., 2009; Maurer et al., 2005;

Penley et al., 2011; Hinman et al., 2011) consistent with a large literature detailing functional and anatomical variation across the septotemporal (anteroposterior in humans) axis (Lavenex & Amaral, 1996). The present study reflects our ongoing analyses to define systematic variation in the theta signals and the underlying mechanisms mediating variation across the long axis of the HPC.

Early work investigating the behavioral correlates of the hippocampal theta signal observed its emergence during locomotion, specifically the running speed of the rodent (Vanderwolf, 1969; Teitelbaum & McFarland, 1971; Whishaw & Vanderwolf, 1973; Feder & Ranck, 1973; McFarland et al., 1975). The increase in theta power as a function of running speed has been established in more recent studies examining the septal pole of the HPC (Rivas et al., 1996; Bouwman et al., 2005) as well as functional differentiation across the longitudinal axis of the HPC (Hinman et al., 2011). Running speed has also been associated with increases in gamma frequency (Ahmed & Mehta, 2012). While Hinman and colleagues demonstrated the systematic decrease in the relationship between speed and theta power across the long axis of the HPC, few studies have detailed variation in whole body acceleration (see however Wyble et al., 2004; Sinnamon, 2000; Gupta et al., 2012). Notably most rodent studies examining cognitive performance involve spatial locomotion often along relatively fixed trajectories (Montgomery et al., 2009) and prototypically involve deceleration within regions of “choice” (often turns), thus a better understanding of the relative contribution of these highly quantifiable variables and their dynamic variation

should facilitate analyses of how variations in theta relate to both sensorimotor and/or cognitive processes.

Materials and Methods

Data used in current analyses was collected as previously described in Hinman and colleagues (2011), thus, briefer descriptions of data collection details are presented below. Key differences relate to data analyses routines and in particular use of data from entirely of data collection trials including stationary and movement periods at each end of the linear track and inclusion of data from 0-30 cm/s (see Fig 1 for distribution of speeds and acceleration values).

Animals and Surgical Procedures

Six Fisher-344 adult male rats, singly housed in a temperature/light controlled environment were used in the present study. All procedures performed were in accordance with the guidelines and regulations implemented by the University of Connecticut's Institutional Animal Care and Use Committee and NIH.

Rats were anesthetized with a ketamine cocktail solution (4 ml/kg consisting of 25 mg/ml ketamine, 1.3 xylazine mg/ml, and 0.25 acepromazine mg/ml). A midline scalp incision was made, burr holes drilled through the skull

over the HPC, and three –four electrode arrays were situated across the septotemporal axis of the HPC. All electrode arrays were comprised of four linearly spaced 50 µm tungsten wires (16 electrodes per animal; California Fine Wire Company, Grover Beach, CA). Electrode wire was arranged and separated by fused silica tubing (Polymicro Tubing, Phoenix, AZ), attached to female pins (Omnetics, Minneapolis, MN) and secured in a rectangular five by four pin array. Two stainless steel watch screws driven into the skull above the cerebellum served as indifferent and ground electrodes. Supplementary anchor screws were positioned anteriorly and the entire headstage ensemble was fortified with dental acrylic. The surgical coordinates, where bregma was used as the reference point, were as follows: Septal HPC (AP -3.0, ML 2.5, DV 3.0); Midseptotemporal HPC (AP -5.0, ML 5.0, DV 5.0); Temporal HPC (AP -6.5, ML 5.5, DV 7.0). After surgery, rats recovered for one week.

Electrophysiological Data Acquisition and Analysis

Details of behavioral paradigm used in this study were as previously described (Hinman et al., 2011). Briefly, animals were trained to run on a 140 cm linear track for a palatable chocolate sprinkle food reward. Recordings required the animal to run 50 trials, where a single trial was denoted as a traversal from one end of the linear track to the other end. Five recording sessions where time was the only manipulation occurred within a single day. All data to be presented was obtained from the first recording session as there is a systematic decrease in the theta signal as a function of repeated behavioral performance within a day

(Hinman et al., 2011).

Wide-band electrical activity was recorded (1-1894 Hz, 3787 samples/sec) using a Neuralynx data acquisition system (Bozeman, MT). During offline analysis, data was down-sampled by a factor of 6, thus changing the sampling rate to 3787/6=~631.167 samples/sec. Electrophysiological recordings occurred during the light phase of the light-dark cycle. Light emitting LEDs attached to the headstage were tracked by a camera (33 samples/sec) situated over the linear track, allowing for a record of the rats' position over time. Speed was calculated by taking the positional difference between successive tracking samples followed by a lowpass filter (cutoff=.25 Hz) in order to minimize the contribution of head movements and other movement artifacts to the overall speed of the animals. Acceleration was calculated by taking the second-order derivative of speed. A representative filtered position versus time trace is shown in Fig. 2A.

Figure 2

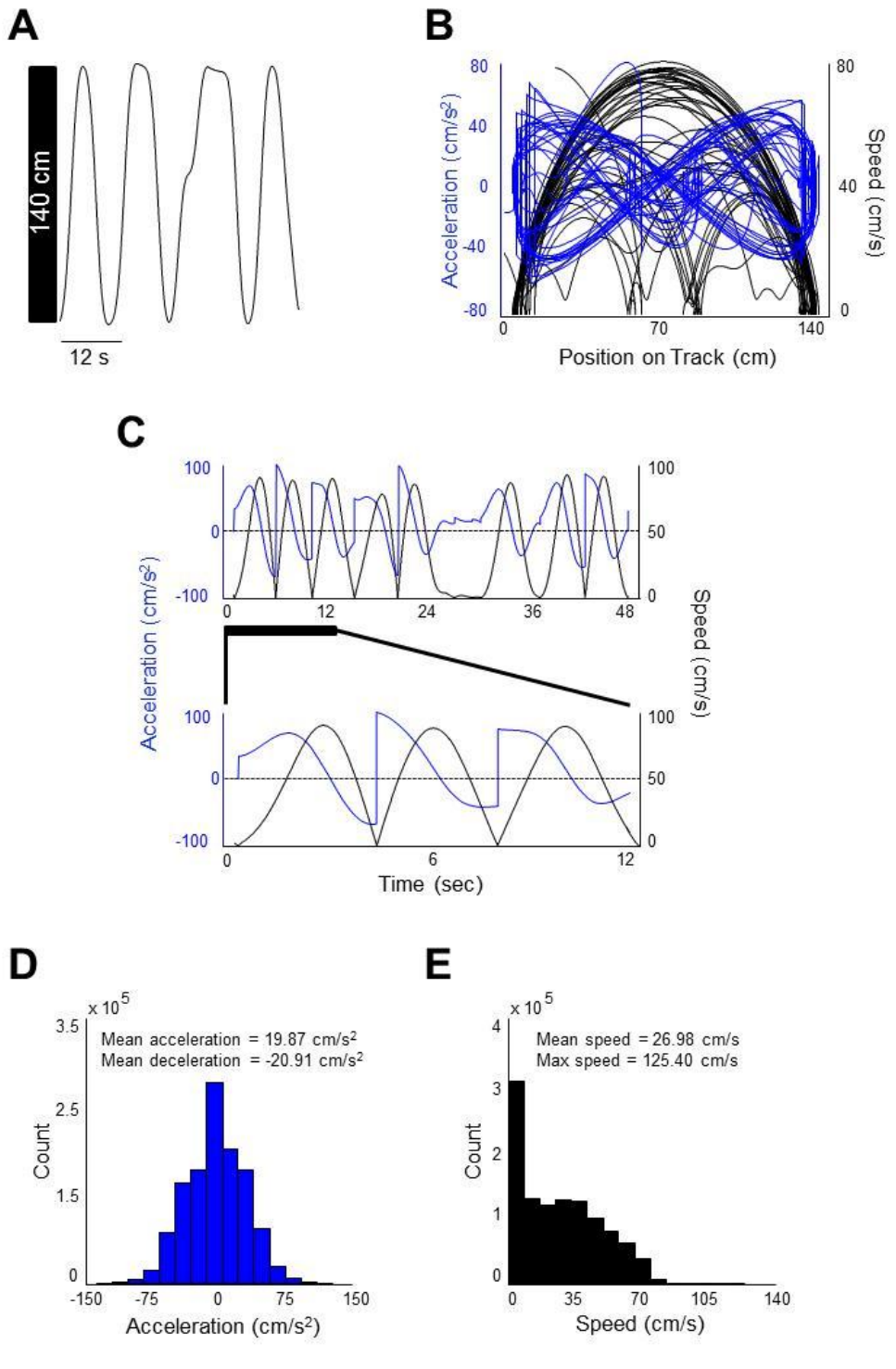
A
140 cm
12 s
B
Acceleration (cm/s²)
Speed (cm/s)
Position on Track (cm)
C
Acceleration (cm/s²)
Speed (cm/s)
Time (sec)
D
x 10^5
Mean acceleration = 19.87 cm/s²
Mean deceleration = -20.91 cm/s²
Count
Acceleration (cm/s²)
E
x 10^5
Mean speed = 26.98 cm/s
Max speed = 125.40 cm/s
Count
Speed (cm/s)

Figure 2. *Methodological specifications*. **A**: The rats' position on the 140 cm length maze (y-axis) over time (x-axis). 8 consecutive trials are shown. **B**: The rats' speed (black) and acceleration (blue) as a function of position on the maze for an entire recording session (~5 minutes). Acceleration is shown in both running directions in order to emphasize the similar distribution of accelerations. **C (top)**: Speed (black) and acceleration (blue) as a function of time. 8 consecutive trials are shown in order to visualize the relationship between speed and acceleration. **C (bottom)**: A closer look at the first 12 seconds of the top signals, now only the first 3 consecutive trials are shown. **D**: Distribution of accelerations for all rats across all recording sessions. Mean acceleration = 19.87 cm/s^2; mean deceleration = -20.91 cm/s^2; max acceleration = 102.70 cm/s^2; max deceleration = -105.74 cm/s^2. **E**: Distribution of speeds for all rats across all recording sessions. Mean speed = 26.98 cm/s; max speed = 125.40 cm/s.

All data analysis were performed using custom written programs in MatLab (The MathWorks, Natick, MA), with some statistical analysis conducted in SPSS (SPSS Inc., Chicago, Illinois). In Fig. 2B a position versus speed (black) and acceleration (blue) trace is visualized as a state-space plot. As described previously, all data was utilized in analyses. The resulting dataset contained an average of 46.4 +/- 0.88 (SEM) trials per recording. The relationship between speed and acceleration is shown in Fig. 2C, while the distribution of speeds and accelerations (positive and negative) for all animals is shown in Fig. 2D and Fig. 2E, respectively. The mean acceleration is 19.87 cm/s^2 with a maximum of 102.70 cm/s^2, while the mean deceleration is -20.91 cm/s^2 with a maximum of -105.74 cm/s^2. Furthermore, the distribution of speeds is shown in Fig. 2E, with a mean speed of 26.98 cm/s and a maximum speed of 125.40 cm/s.

Spectral Indices & Statistics

For each recording, all data was used and theta envelopes were calculated as an instantaneous measure of theta amplitude. Theta phase was obtained from the Hilbert transform of the theta (6-12 Hz) bandpass filtered signal and then the instantaneous frequency was calculated by taking the change in phase divided by the change in time between each sample.

The instantaneous envelope amplitude from each electrode was subjected to a multiple regression analysis that included the speed, acceleration and the interaction between the two (speed x acceleration) in order to assess the

relationship between locomotor speed, acceleration and theta amplitude. Thus, each electrode yielded a standardized regression coefficient value (beta, β where $\beta = b\frac{SD_x}{SD_y}$) that assessed the linear association between speed, acceleration, and the interaction of theta envelope by speed/acceleration. Beta coefficients standardize predictor variables such that their variances equal one. Similar to z-scores, beta coefficients describe how many standard deviations a dependent variable (in this case theta amplitude) will change in response to a standard deviation increase in a given predictor variable. Thus, beta coefficients describe which independent variable has a greater effect on the dependent variable. A non-significant beta coefficient indicates that a predictor variable does not significantly contribute to explaining variability in the dependent variable. A representative model for the prediction of theta amplitude might look something like this:

$$\theta amplitude = Speed(\beta speed) + Accel(\beta Accel) + Interaction(\beta Interaction)$$

where each beta-value for a given electrode can be inserted into the model to accurately predict theta amplitude.

Beta coefficients obtained from the multiple regression indicate which predictor has a greater effect on the dependent variable, but does not indicate if the independent variables are correlated (co-vary) with each other. In order to partial out the contribution of one independent variable to another, partial correlations were calculated. Thus, squared partial correlations may be understood best as the proportion of variance not associated with other

independent variables and that is associated with the independent variable of interest. Partial correlations can be understood as the correlation between the residuals R_X and R_Y, which are a result from the linear regression of predictor X with dependent variable Z and predictor Y with dependent variable Z. Simply put, the partial correlation can be calculated by solving the two associated linear regression problems, find the residuals, and then calculate the correlation between the residuals. If a predictor significantly contributes to explaining variability in the dependent variable, as indicated by a significant beta (β) coefficient in the multiple regression model(s), that predictor was added to the partial correlation analysis.

For the partial correlation, acceleration was divided into one of 3 categories 1) all acceleration [positive and negative taken together] 2) positive acceleration (acceleration) and 3) negative acceleration (deceleration). The corresponding theta amplitude was indexed for each acceleration category and was added to the partial correlation model. Since zero acceleration can be denoted as no movement (stopped at end of trial) or constant movement (eg: 60 cm/s, with no acceleration), these data points were not included in analyses. Furthermore, these data points have little influence or contribution to the overall model due to their low values (see model above).

Electrodes within each septotemporal extent of DG and CA1 (Fig. 2A) were separately grouped in order to determine whether that areal region had a mean partial correlation (speed/acceleration) value that is different than zero using a single-sample t-test. A significant non-zero mean for a particular areal

speed/acceleration partial correlation value indicates that theta amplitude is significantly speed and/or acceleration modulated in either the positive or negative direction (Lorch & Myers, 1990). Furthermore, a simple linear correlation was conducted on the partial correlation values for areal regions accompanied by distance from the septal pole (millimeters) as an explanatory variable, allowing for the demonstration of whether speed and acceleration modulation of theta amplitude/frequency varied across the septotemporal axis. In order to assess if there was a significant difference in the relationship between acceleration and theta amplitude and deceleration and theta amplitude and or differences in modulation of theta amplitude by acceleration in different hippocampal subregions (eg, CA1 vs DG), a paired-samples t-test was conducted. A significant test statistic indicates that the relationship between theta amplitude and acceleration/deceleration is differentially modulated.

Histology

Histological procedures have been explained elsewhere (Hinman et al., 2011). Briefly, animals were transcardially perfused with ice-cold saline followed by 4% paraformaldehyde in .1M phosphate buffer. Brains were sliced using a vibratome, mounted, and Nissl stained using thionin. Septotemporal distances between electodes were verified by placing each electrode position on a flatmap representation of the HPC (Fig. 2A; Swanson et al., 1978). Photomicrographs of electrode tracks were taken, digitized and prepared for presentation.

Figure 3

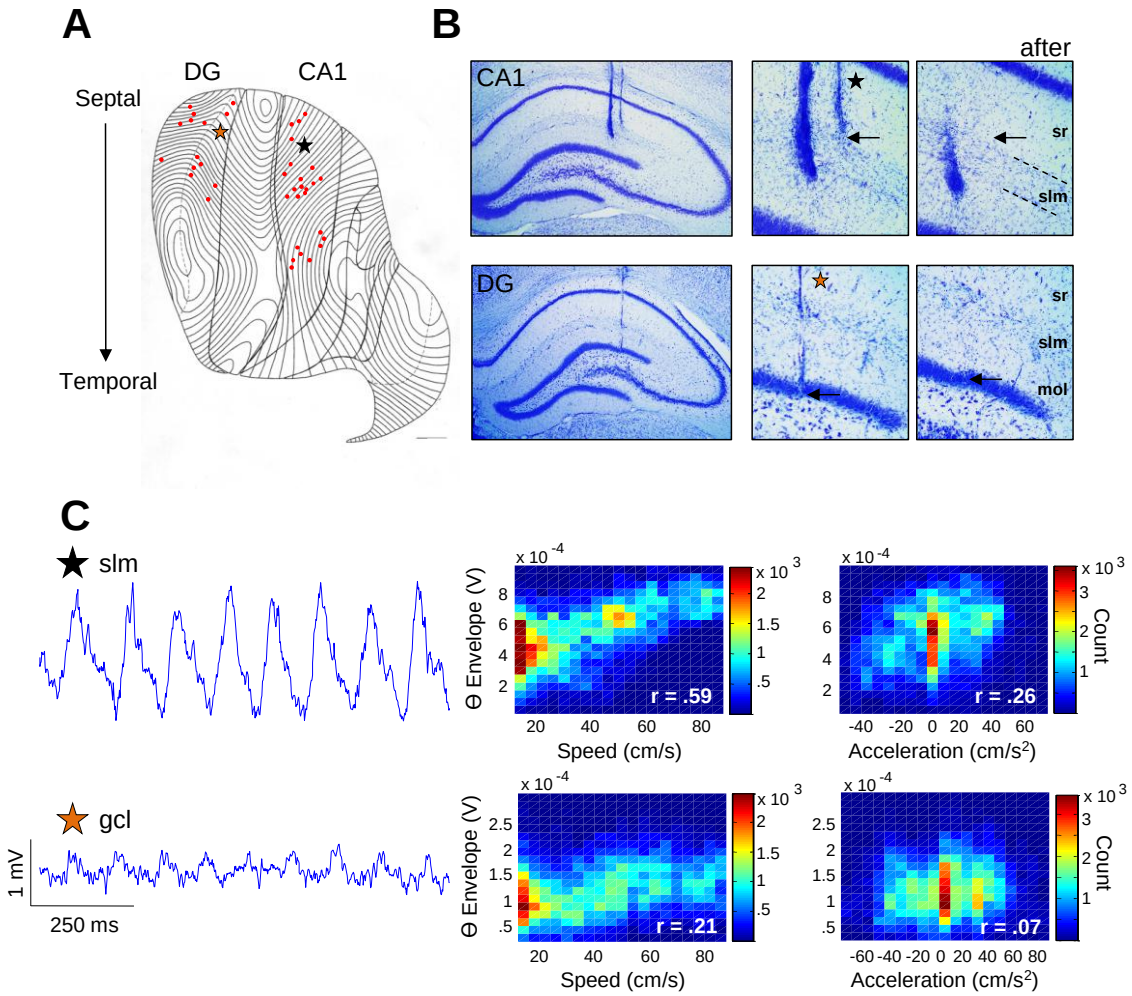
A
DG
CA1
Septal
Temporal
B
after
CA1
DG
sr
slm
mol
C
slm
gcl
1 mV
250 ms
Θ Envelope (V)
Speed (cm/s)
r = .59
Acceleration (cm/s²)
r = .26
r = .21
r = .07
Count

Figure 3. *Electrode locations and corresponding theta traces.* **A**: Flatmap representation of the hippocampal formation. Electrode placements are denoted by red dots. The septal pole is at the *top* and the temporal pole is at the *bottom*. Each contour line represents a coronal section that has been unfolded and placed on a two-dimensional plane. Orange star denotes DG electrode as in B (bottom), while black star denotes CA1 electrode as in B (top). **B (top)**: Photomicrographs of representative recording sites in septal CA1. Middle photomicrograph shows a close-up (20x) of where the electrode tip ends, as denoted by the black arrow. The right photomicrograph shows the next coronal section after the end of the electrode placement for verification that the electrode tract does not continue. The septal CA1 tract ends in slm (stratum lacunosum moleculare). **B (bottom)**: Same as top, but for DG. The septal DG tract ends in the gcl (granule cell layer). **C (left, top)**: Raw theta trace from representative CA1 slm electrode, as depicted in B (top, black star). **C (right, top)**: corresponding speed to amplitude and acceleration to amplitude relationship for the same representative CA1 slm electrode. **C (left, bottom)**: Same as for CA1, but for DG. From visual inspection alone, differences between CA1 and DG are apparent. ***Abbreviations***: sr=stratum radiatum; slm=stratum lacunosum moleculare; mol=molecular layer; gcl=granule cell layer.

Results

Histological verification was as previously reported (Hinman et al., 2011) and confirmed that the majority of sites were positioned in stratum radiatum of CA1 (N=27) sites; additional sites within CA1 spanned from the ventral aspect of stratum pyramidale to stratum lacunosum moleculare. DG (N=15) sites were mainly positioned in stratum granulosum (Fig. 3A). With regards to septotemporal position, CA1 sites spanned from 1.3 - 7.6 mm along the long axis, while DG sites were more narrow and spanned from 1.4 - 4.8 mm (septal and mid-septotemporal regions). Photomicrographs show septal CA1 (top) and DG (bottom) placements and the following coronal section after the end of the electrode tip in order to confirm its termination (Fig. 3B). For photomicrographs of temporal HPC placements, refer to Hinman et al., 2011. Representative theta traces are shown in Fig. 3C for the electrodes in Fig 3B, as denoted by colored stars. Speed to theta amplitude and acceleration to theta amplitude two-dimensional histograms are shown on the right for corresponding electrodes. Two-dimensional histograms represent the joint distribution of variables X and Y and are thus color-coded according to the number of occurrences where Y (eg, theta amplitude) is a particular value at a given X (eg, speed, acceleration) value. Warmer colors (eg, red) signify that there are a higher number of occurrences where Y is a particular value at a given X value. For a clearer interpretation, two-dimensional histograms can best be understood and visualized as a scatter-plot with an overlaid grid, where the numbers of points are counted within the grid and represented on a color scale.

Theta amplitude varied as a function of laminar position in septal HPC, as has been well-documented elsewhere (Bragin et al., 1995). Sites nearest stratum lacunosum moleculare of CA1 and stratum moleculare of the DG yielded the greatest amplitude signals (Fig. 3C). Differences in theta amplitude could reflect variation in afferent input, the density of afferent input that are participating in LFP generation, and/or the density of dendritic innervation in which those afferents terminate.

The effect of speed and all acceleration (positive & negative taken together) on theta amplitude

The current data set included the entirety of each recording session (roughly 2-3 minutes of continuous recording). Thus, the data included a wider distribution of speeds and similarly acceleration values. It is important to note that the data set as presented by Hinman et al., 2011, isolating the last 1.5 seconds of each traversal, was skewed with regards to negative acceleration (deceleration) values. The distribution of speed and acceleration values for all animals is shown in Figure 2D and 2E, respectively.

Even with the inclusion of a wider range of speed and acceleration values, the current data set exhibited a significant difference in speed modulation of theta amplitude only in septal CA1 (data not shown; septal $t(5) = 24.987$ $p = .0001$; midseptotemporal $t(13) = .117$ $p = .909$ n.s.; temporal $t(7) = -1.477$ $p = .183$ n.s.) as compared to Hinman et al., 2011. With regards to DG, there was no

significant difference in speed modulation of theta amplitude at any septotemporal extent (data not shown; septal t(7) = -1.545 p = .166 n.s.; midseptotemporal t(6) = -1.028 *p* = .343 n.s.).

Upon inspection of the relationship between all acceleration (positive and negative taken together) and theta amplitude for a CA1 septal electrode the relationship appears nonlinear (Fig. 4A right) and for comparison, the same CA1 septal electrode is displayed showing the relationship between speed and theta amplitude (Fig. 4A left). Each septotemporal position was significantly modulated by speed in CA1 (Fig. 4B top gray bars; septal t(4) = 10.93, *p* = .0003; midseptotemporal t(13) = 5.12 *p* = .0002; temporal t(7) = 3.77 *p* = .007) and DG with the exception of mid DG (Fig. 3B bottom gray bars; septal t(7) = 6.92, *p* = .0002; midseptotemporal t(6) = .78 *p* = .464 n.s.).

Each septotemporal position was significantly modulated by all acceleration in CA1, with the exception of temporal CA1 (Fig. 4B top black bars; septal t(4) = 4.50 *p* = .011; midseptotemporal t(13) = 4.38 *p* = .001; temporal t(7) = 1.13 *p* = .297 n.s.) and DG (Fig. 3B bottom black bars; septal t(7) = 2.55 *p* = .038; midseptotemporal t(6) = 4.70 *p* = .003). Furthermore, the relationship between acceleration and theta amplitude decreased across the long axis of CA1 (Fig. 4C top black circles; r =-.44 *p* = .021), but not in DG (Fig. 34 bottom black circles; r =.16 *p* = .561 n.s.). Each point in the scatter plots represents a partial correlation value for the relationship between, for example, speed and theta amplitude (controlling for all acceleration) for a particular electrode as a function of distance from the septal pole.

Figure 4

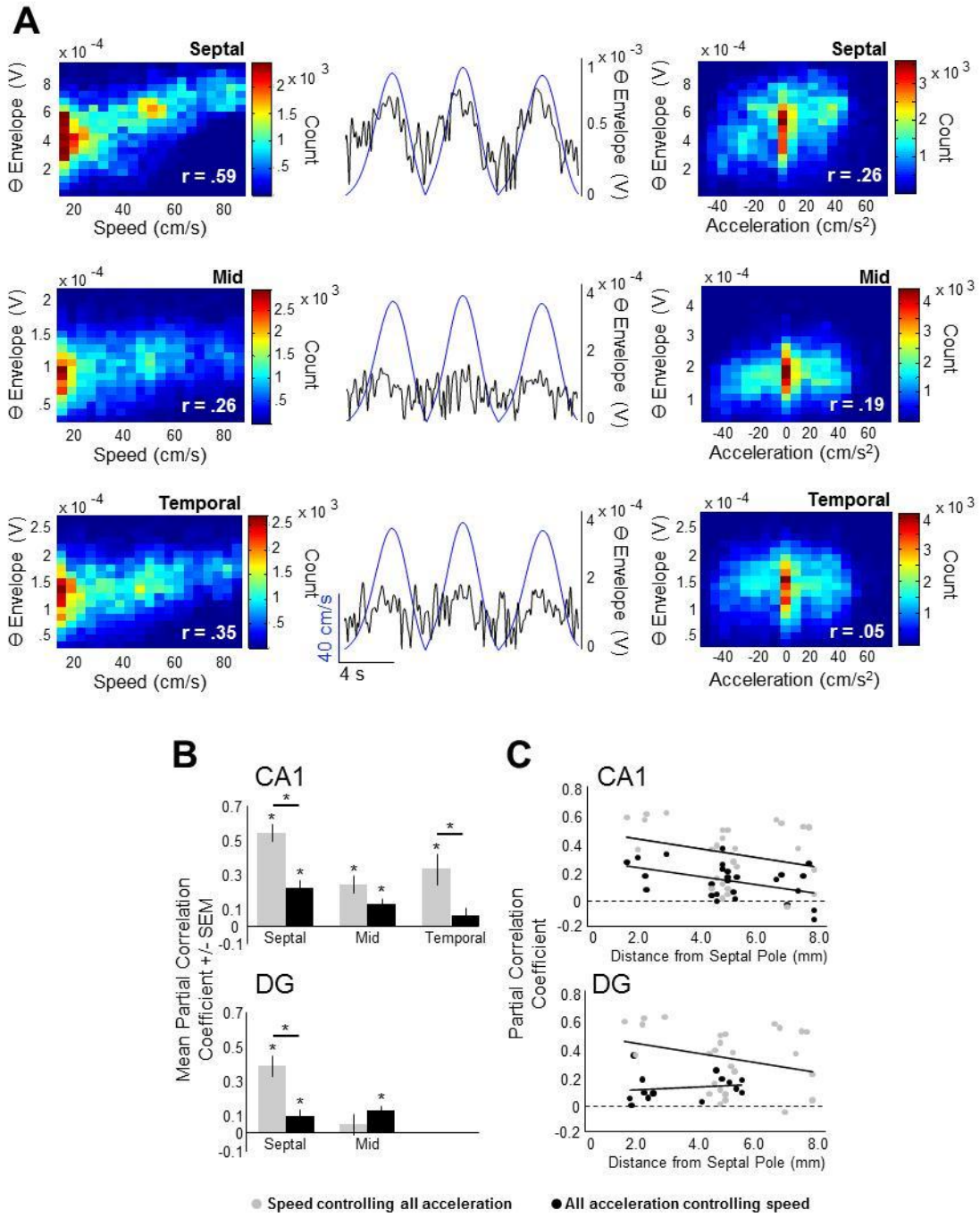
A
Septal
Mid
Temporal
Θ Envelope (V)
Count
Speed (cm/s)
Acceleration (cm/s²)
r = .59
r = .26
r = .35
r = .26
r = .19
r = .05
40 cm/s
4 s
B
CA1
DG
Mean Partial Correlation Coefficient +/- SEM
Septal
Mid
Temporal
C
Partial Correlation Coefficient
Distance from Septal Pole (mm)
Speed controlling all acceleration
All acceleration controlling speed

Figure 4. *Relationship between speed, acceleration and theta amplitude across the long axis of the hippocampus*. **A (*left*)**: two-dimensional histograms (joint histograms, or color coded scatterplots) of the relationship between speed and theta amplitude across the septotemporal axis of the hippocampus for simultaneously recorded CA1 electrodes. Each color pixel represents the number of occurrences with a specified speed (or acceleration, x-axis) at a particular theta amplitude (y-axis). **A (*middle*)**: Speed modulation (blue) of theta envelope (black) over time across the septotemporal axis of CA1 for the same simultaneously recorded CA1 electrodes as shown on the left. Three consecutive trials are shown. By visual inspection alone it becomes apparent that speed modulation of theta amplitude decreases across the longitudnal axis. **A (*right*)**: Same as left figures, but now for acceleration. Two-dimensional histograms of the relationship between acceleration (positive and negative taken together) and theta amplitude across the septotemporal axis of the hippocampus for the same simultaneously recorded CA1 electrodes as shown on the left. **B**: All CA1 (top) and DG (bottom) electrodes were grouped according to septotemporal position in order to assess the relationship between speed, acceleration and theta amplitude across the long axis of the hippocampus. The mean partial correlation coefficients for speed controlling for acceleration (gray) and acceleration controlling for speed (black) across the longitudinal axis are shown. Theta amplitude was significantly speed modulated across the entirety of the hippocampus in CA1 and only in septal DG (**P* < 0.01, t-test). Theta amplitude was also significantly modulated by acceleration in septal and midseptotemporal regions of CA1 and DG (**P* < 0.05, t-test). Additionally, speed is a better predictor of theta amplitude than acceleration in septal and temporal regions of CA1 *(*P* < 0.05, t-test), and only in septal DG (*P* < 0.01). **C**: Partial correlation coefficients for the relationship between speed and theta amplitude (gray) and acceleration and theta amplitude (black) as a function of distance from the septal pole for CA1 (top) and DG (bottom). Each dot represents the partial correlation coefficient between each index (speed, acceleration) and theta amplitude and plotted as a function of distance from the septal pole.

Moreover, there were no differences in septal CA1 vs, DG sub-regions for speed modulation of theta amplitude (Fig 4B gray bars; t(11) = 1.743 *p* = .109 n.s.) but there was a significant difference in in CA1 and DG in midseptotemporal extents (Fig 4B gray bars; t(19) = 2.44 *p* = .025). Furthermore, there were no significant differences between hippocampal sub-regions across the areal axis for the relationship between acceleration and theta amplitude modulation (Fig 4B black bars; septal; t(11) = 1.872 *p* = .088 n.s.; midseptotemporal ; t(19) = -.067 *p* = .947 n.s.).

These data suggest that over and above speed, acceleration significantly contributes to explaining variability in theta amplitude in CA1 and DG, and this relationship decreases across the septotemporal axis of CA1. Taken together, acceleration accounted for a significant portion of the variability in theta amplitude at septal most sites, while sites located more temporally displayed a decrease in the relationship between acceleration and theta amplitude in CA1 but not DG.

The effect of acceleration and deceleration on theta amplitude

As stated earlier, the relationship between acceleration and theta amplitude appears to be non-linear and quadratic (Fig. 5A). Because of this relationship, we divided acceleration into its positive (Fig. 5A, right) and negative (Fig. 5A, left) constituents, as shown by this septal CA1 example. The mean partial correlation coefficient for all septal CA1 electrodes for negative

acceleration (deceleration, blue) and positive acceleration (acceleration, red) is significantly different than zero (Fig. 5B; deceleration t(4) = 19.44 p = .00004; acceleration t(4) = -2.98 p = .041), with deceleration explaining more variability in theta amplitude variability than acceleration. For ease of presentation, since the relationship between positive acceleration (acceleration) and theta amplitude is negative, we "rectified" this non-linearity by taking the absolute value of the mean partial correlation coefficients for the relationship between acceleration and theta amplitude. (Fig. 5B; right red bar). All partial correlation coefficient means and scatter plot values associated with positive acceleration have been rectified unless otherwise denoted. All septotemporal positions in CA1 exhibit both deceleration and acceleration modulation of theta amplitude that is significantly different from zero (Fig. 5C top; septal CA1 deceleration (blue bars) t(4) = 19.44 p = .0002 acceleration (red bars) t(4) = -2.982 p = .041; midseptotemporal deceleration t(13) = 10.619 p < .0001 acceleration t(13) = -5.912 p = .00005; temporal deceleration t(7) = 3.986 p = .005 acceleration t(7) = -6.464 p = .0003). DG shows the same relationship as CA1 (Fig. 5C bottom; septal DG deceleration (blue bars) t(7) = 5.45 p = .001 acceleration (red bars) t(7) = -.8102 p = .0008; midseptotemporal deceleration t(6) = 5.884 p = .001 acceleration t(6) = -4.455 p = .004). Moreover, there is a significant difference in the relationship between deceleration and theta amplitude and acceleration and theta amplitude in all but temporal levels of CA1 (Fig. 5C top; septal t(4) = -5.305 p = .006; midseptotemporal t(13) = -5.274 p = .0001; temporal t(7) = -1.172 p = .279 n.s.) as well as for DG (Fig, 5C bottom; septal t(7) = -3.519 p = .01; midseptotemporal

t(6) = -5.350 *p* = .002). Further, the relationship between deceleration and theta amplitude decreases across the long axis of CA1 (Fig. 5D top blue circles; r = -.709 *p* = .00004) but not DG (Fig. 5D bottom blue circles; r = -.074 *p* = .792 n.s.), while the relationship between acceleration and theta amplitude remains constant across the septotemporal axis of CA1 (Fig. 5D top red circles; r = .-216 *p* = .279 n.s.) but increases across the septotemporal axis of DG (Fig. 5D bottom red circles; r = .532 *p* = .041). Note that negative partial correlation values for the scatter plots were rectified in order to observe the strength of the correlation regardless of direction. Each point on the scatter plots represents the partial correlation coefficient between, for example, deceleration and theta amplitude controlling for speed as a function of distance from the septal pole.

Figure 5

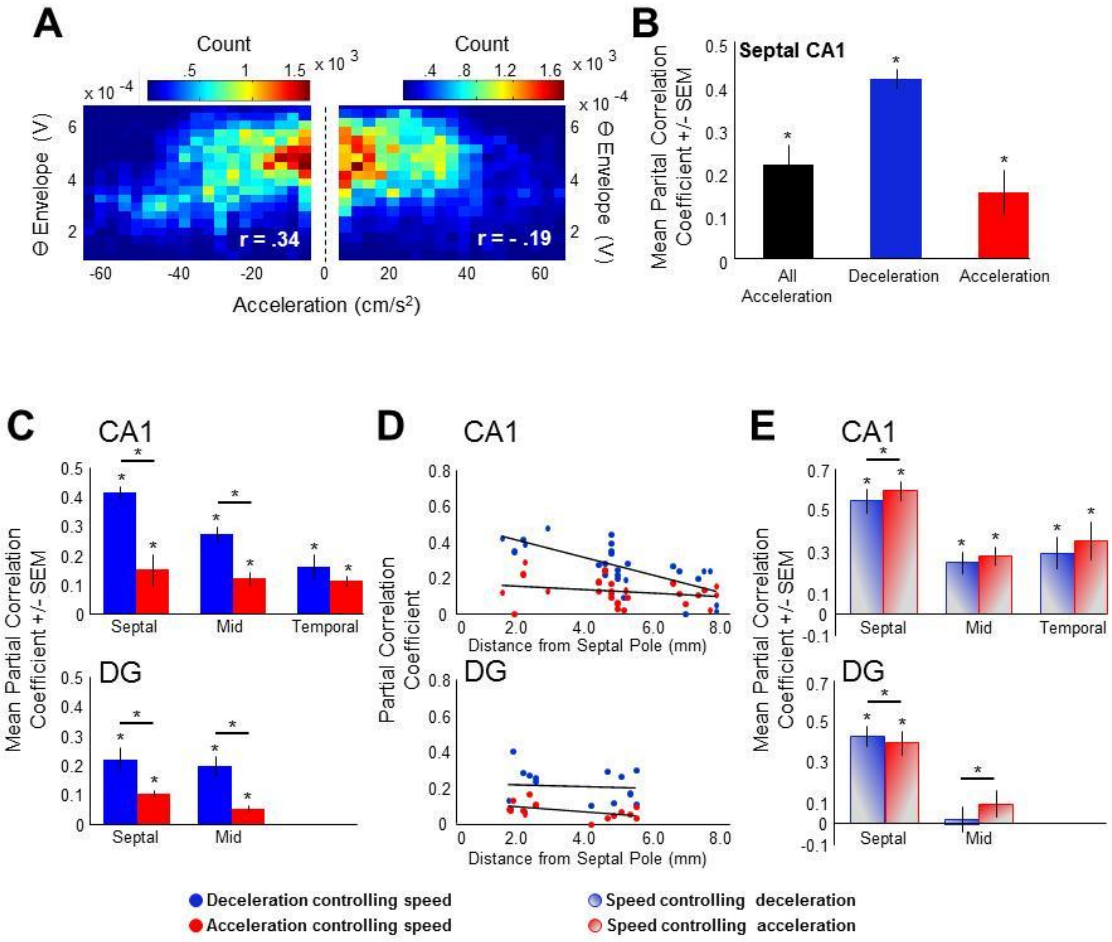
A
Count
.5 1 1.5 x 10 3
x 10 -4
Θ Envelope (V)
6
4
2
r = .34
-60 -40 -20 0
Count
.4 .8 1.2 1.6 x 10 3
x 10 -4
Θ Envelope (V)
r = - .19
20 40 60
Acceleration (cm/s²)
B
Septal CA1
Mean Partial Correlation Coefficient +/- SEM
0.5 0.4 0.3 0.2 0.1 0
All Acceleration
Deceleration
Acceleration
C
CA1
Mean Partial Correlation Coefficient +/- SEM
0.5 0.4 0.3 0.2 0.1 0
Septal
Mid
Temporal
DG
Septal
Mid
D
CA1
Partial Correlation Coefficient
0.8 0.6 0.4 0.2 0
0 2.0 4.0 6.0 8.0
Distance from Septal Pole (mm)
DG
Distance from Septal Pole (mm)
E
CA1
Mean Partial Correlation Coefficient +/- SEM
0.7 0.5 0.3 0.1 0 -0.1
Septal
Mid
Temporal
DG
Septal
Mid
Deceleration controlling speed
Acceleration controlling speed
Speed controlling deceleration
Speed controlling acceleration

Figure 5. *Relationship between acceleration, deceleration and theta amplitude*. **A *(left)***: two-dimensional histograms of the relationship between deceleration and theta amplitude for a representative septal CA1 electrode. **A (*right*)**: same as left figure, but for acceleration. **B**: Mean partial correlation coefficients (controlling for speed) for the relationship between all acceleration (black bar, positive and negative taken together) and theta amplitude, deceleration (blue bar, deceleration) and acceleration (red bar) and theta amplitude for all septal CA1 electrodes. The relationship between acceleration and theta amplitude is negative (mean partial correlation coefficient = -.15). For clearer interpretation the non-linearity was rectified by taking the absolute value of the negative mean partial correlation coefficient between acceleration and theta amplitude. The absolute value is shown, unless otherwise specified. As can be seen, when acceleration is separated into its positive and negative constituents, a differential relationship emerges such that deceleration is more predictive of theta amplitude as compared to acceleration. **C**: All CA1 (top) and DG (bottom) electrodes were grouped according to septotemporal position in order to assess the relationship between acceleration, deceleration and theta amplitude across the long axis of the hippocampus. The mean partial correlation coefficients for deceleration and theta amplitude controlling for speed (blue bars) and acceleration and theta amplitude controlling for speed (red bars) across the longitudinal axis are shown. Again, the absolute value of the mean partial correlation coefficient between acceleration and theta amplitude was taken. Theta amplitude was significantly modulated by both acceleration and deceleration across the entirety of the hippocampus for both CA1 and DG sites (*P < 0.01, t-test). Additionally, deceleration explained more of the variability in theta amplitude across septal and midseptotemporal levels of CA1 and DG axes (*P < 0.01, t-test). **D**: Partial correlation coefficients for the relationship between deceleration and theta amplitude (blue circles) and acceleration and theta amplitude (red circles) as a function of distance from the septal pole for CA1 (top) and DG (bottom). Each dot represents the partial correlation coefficient between each index (acceleration, deceleration) and theta amplitude plotted as a function of distance from the septal pole. The relationship between deceleration and theta amplitude decreased across the septotemporal axis of CA1 (*P < 0.05, correlation), but not DG (*P > 0.05, correlation), while the relationship between acceleration and theta amplitude remained constant across the long axis of CA1 (*P > 0.05, correlation), but increased across the long axis of DG (*P < 0.05, t-test, correlation). Note that negative partial correlation values for the scatter plots were rectified, thus the relationship between theta amplitude and acceleration actually increased across the long axis, not decreased, as what is depicted. **E**: Mean partial correlation coefficients for the relationship between speed and theta amplitude during deceleration (faded blue bar) and acceleration (faded red bar). The relationship between speed and theta amplitude is differentially modulated during acceleration and deceleration in septal CA1 and across the entirety of the long axis of DG (*P < 0.05).

Moreover, the speed to theta amplitude relationship during acceleration and deceleration is significantly different than zero at all septotemporal extents of CA1 (Fig. 5E top; septal CA1 speed to amplitude during deceleration, faded blue bars $t(4) = 9.321$ $p = .001$ speed to amplitude during acceleration, faded red bars $t(4) = 13.369$ $p = .0002$; midseptotemporal deceleration $t(13) = 4.779$ $p = .0004$ acceleration $t(13) = 6.433$ $p = .00002$; temporal deceleration $t(7) = 3.932$ $p = .006$ acceleration $t(7) = 3.989$ $p = .005$) and septal parts of DG (Fig. 5E bottom; septal DG deceleration, faded blue bars $t(7) = 8.311$ $p = .00007$ speed to amplitude during acceleration, faded red bars $t(7) = 6.738$ $p = .0003$; midseptotemporal deceleration $t(6) = .384$ $p = .714$ n.s. acceleration $t(6) = 1.518$ $p = .180$ n.s.). Further, there is a significant difference in the modulation of theta amplitude by speed during acceleration and deceleration in septal CA1 (Fig. 5E top; septal CA1 $t(4) = 3.015$ $p = .039$; midseptotemporal $t(13) = 1.633$ $p = .126$ n.s.; temporal $t(7) = 2.115$ $p = .072$ n.s.) and at septal and midseptotemporal sites of DG (Fig. 5E bottom; septal DG $t(7) = -2.475$ $p = .042$; midseptotemporal $t(6) = 2.957$ $p = .025$).

Overall there is a differential relationship between theta amplitude and acceleration/deceleration, with deceleration explaining more of the variability in theta amplitude as compared to acceleration. Furthermore, the relationship between all acceleration and theta amplitude appears to be non-linear, with the relationship between theta amplitude and deceleration being highly positive, while the relationship between acceleration and theta amplitude is negative (note rectification, as previously described). Moreover, the relationship between

deceleration and theta amplitude decreases across the septotemporal axis of CA1, but not DG, while the relationship between acceleration and theta amplitude shows the opposite effect – it decreases across the long axis of DG, but not CA1. Lastly, the modulation of theta amplitude by speed during acceleration and deceleration is different at septal sites of CA1 and DG as well as midseptotemporal sites of the DG.

Moreover, there was a significant difference in CA1 and DG in modulation of theta amplitude by acceleration at midseptotemporal extents (Fig 5C red bars; $t(19) = -2.312$ $p = .032$), while septal extents displayed no differences between DG and CA1 (Fig 5C red bars; $t(11) = -1.137$ $p = .280$ n.s.). There was a significant difference in CA1 and DG in modulation of theta amplitude by deceleration at septal extents (Fig 5C blue bars; $t(11) = 3.525$ $p = .005$), while midseptotemporal extents displayed no difference (Fig 5C blue bars; $t(19) = 1.68$ $p = .109$ n.s.). Furthermore, the speed to amplitude relationship during acceleration in CA1 and DG was significantly different in septal (Fig. 5E faded red bars; $t(11) = 2.44$ $p = .033$) and midseptotemporal extents (Fig. 5E; $t(19) = 2.394$ $p = .027$), while deceleration showed a differential modulation of theta amplitude in CA1 and DG at only midseptotemporal extents (Fig. 5E faded blue bars; septal $t(11) = 1.485$ $p = .166$ n.s.; midseptotemporal $t(19) = 2.61$ $p = .017$).

Figure 6 summarizes findings as described above. Fig. 6A shows a three-dimensional scatter plot with position on the maze on the x-axis, speed on the y-axis and color –coded for theta amplitude. As can be seen, theta amplitude is highest in the center of the maze, where animal speeds are maximal. Further

inspection of the non-linear relationship between acceleration and theta amplitude demonstrates that at high accelerations (Fig. 6B red scatter plot) and high decelerations (Fig. 6B blue scatter plot), theta amplitude is low and increases in amplitude as a function of less extreme accelerations (both negative and positive, Fig. 6B). Just as in Figure 6A, position on maze is on the x-axis, speed on the y-axis and color-coded for theta amplitude. Data presented is for acceleration (positive and negative) in one direction (rat moving rightwards). Additional examination of the relationship between speed, acceleration and theta amplitude further demonstrates the "shunting" of theta amplitude at high accelerations and decelerations, although more pronounced at high decelerations (Fig. 6C). The purple starts denote maximal acceleration, while the green stars represent maximal decelerations.

Figure 6

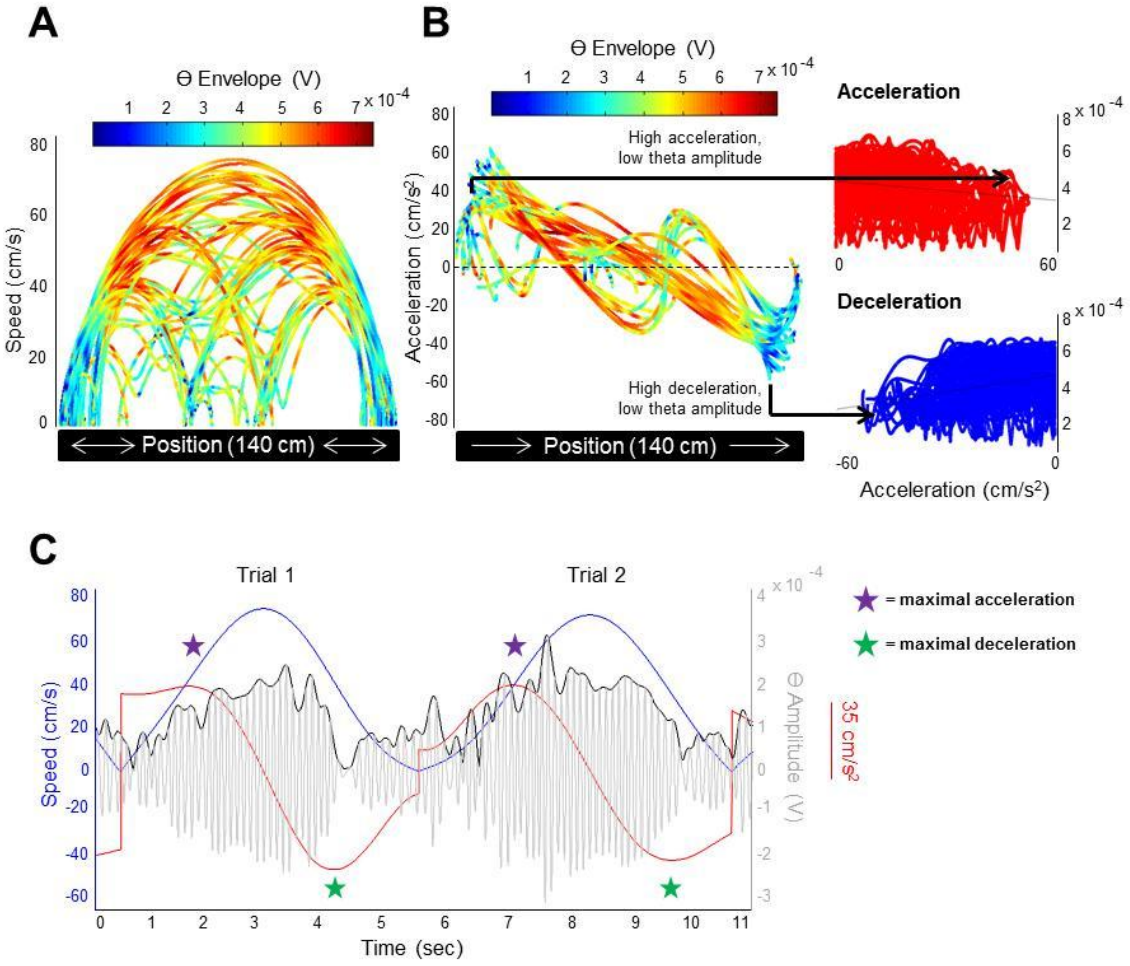
A
Θ Envelope (V)
1 2 3 4 5 6 7 x 10-4
Speed (cm/s)
80
60
40
20
0
Position (140 cm)
B
Θ Envelope (V)
1 2 3 4 5 6 7 x 10-4
Acceleration (cm/s2)
80
60
40
20
0
-20
-40
-60
-80
High acceleration, low theta amplitude
High deceleration, low theta amplitude
Position (140 cm)
Acceleration
Deceleration
8 x 10-4
6
4
2
0
60
-60
Acceleration (cm/s2)
C
Trial 1
Trial 2
= maximal acceleration
= maximal deceleration
Speed (cm/s)
Θ Amplitude (V)
x 10-4
35 cm/s2
Time (sec)
0 1 2 3 4 5 6 7 8 9 10 11

Figure 6. *Speed, acceleration and theta amplitude as a function of position on the maze*. **A**: Three-dimensional scatterplot showing the relationship between position on the maze (x-axis), speed (y-axis), and color-coded for theta amplitude. The maze is 140 cm long. As can be seen, with increasing and maximal speeds (centered in the middle of the maze) theta amplitude increases. **B**: Same as A, but for acceleration in one direction (rat moving rightwards) as denoted by the white arrows on the x-axis. At high positive accelerations (red scatter plot) and high negative accelerations (blue scatter plot) theta amplitude is low and increases in amplitude at less extreme accelerations. **C**: Filtered theta signal (gray) and theta envelope (black) plotted along with speed (blue) and acceleration (red). As can be seen, there is a "shunting" of the theta amplitude at extreme accelerations and decelerations, and is more pronounced at high decelerations, as represented by the three-dimensional scatter plot in B. Purple stars represent time points of maximal acceleration, while green stars represent points of maximal deceleration.

The effect of acceleration and deceleration on theta frequency

The relationship between theta frequency and acceleration was investigated by the same means as the relationship between theta amplitude and acceleration, as described above. Theta frequency increased as a function of all acceleration, as shown by an individual septal CA1 example (Fig. 7B). The relationship between speed and theta frequency for a representative septal CA1 electrode is shown for comparison (Fig. 7A). Further, the mean partial correlation coefficients for all acceleration (positive and negative taken together) were significantly different than zero at all septotemporal levels of CA1 (data not shown; septal $t(4) = 9.340$ $p = .001$; midseptotemporal $t(13) = 10.735$ $p < .0001$; temporal $t(7) = 8.438$ $p = .00006$) and DG (data not shown; septal $t(7) = 3.609$ $p = .009$; midseptotemporal $t(6) = 2.883$ $p < .028$). Just as for theta amplitude, we separated acceleration into its positive (acceleration; Fig 7B, right) and negative (deceleration; Fig 7B, left) constituents. Controlling for the influence of speed, the mean partial correlation coefficient for the relationship between theta frequency and deceleration is significantly different than zero for CA1 electrode sites (Fig. 7C top blue bars; septal $t(4) = 8.657$ $p = .001$; midseptotemporal $t(13) = 9.183$ $p < .0001$; temporal $t(7) = 7.103$ $p = .0002$) as well as for DG electrodes (Fig. 7C bottom blue bars; septal $t(7) = 2.622$ $p = .034$; midseptotemporal $t(6) = 2.460$ $p = .049$). Thus, theta frequency was positively modulated by deceleration of the animal in all regions of the HPC explored, where deceleration was more predictive of theta frequency as compared to acceleration, similar to the theta amplitude data as presented earlier. Additionally, the relationship between

positive acceleration (acceleration) and theta frequency is only significant in temporal CA1 extents of the HPC (Fig. 7C top gray bars; septal t(4) = 1.707 *p* = .163 n.s.; midseptotemporal t(13) = 1.871 *p* = .084 n.s.; temporal t(7) = 2.739 *p* = .029), while there is no significant relationship between acceleration and theta frequency in any areal region of DG (Fig. 7C bottom gray bars; septal t(7) = 2.339 *p* = .052 n.s.; midseptotemporal t(6) = -1.068 *p* = .327n.s.). In the case of theta frequency and acceleration, the relationship is not negative (eg: mean partial correlation coefficients above zero) as it is between theta amplitude and acceleration, thus, no rectification process (absolute value) was needed. Therefore, all partial correlation coefficient means for acceleration and theta frequency were not manipulated. Furthermore, the relationship between deceleration and theta frequency decreased across the septotemporal axis in CA1 (Fig. 7D top blue circles; r = -.667 *p* = .0001) but not in DG (Fig. 7D bottom blue circles; r = -.16 *p* = .569 n.s.). The relationship between positive acceleration and theta frequency remained constant across the long axis of CA1 (Fig 7D top gray circles; r = .238 *p* = .233 n.s.) but decreased across the long axis of DG (Fig. 7D bottom gray circles; r = -.57 *p* = .027).

Figure 7

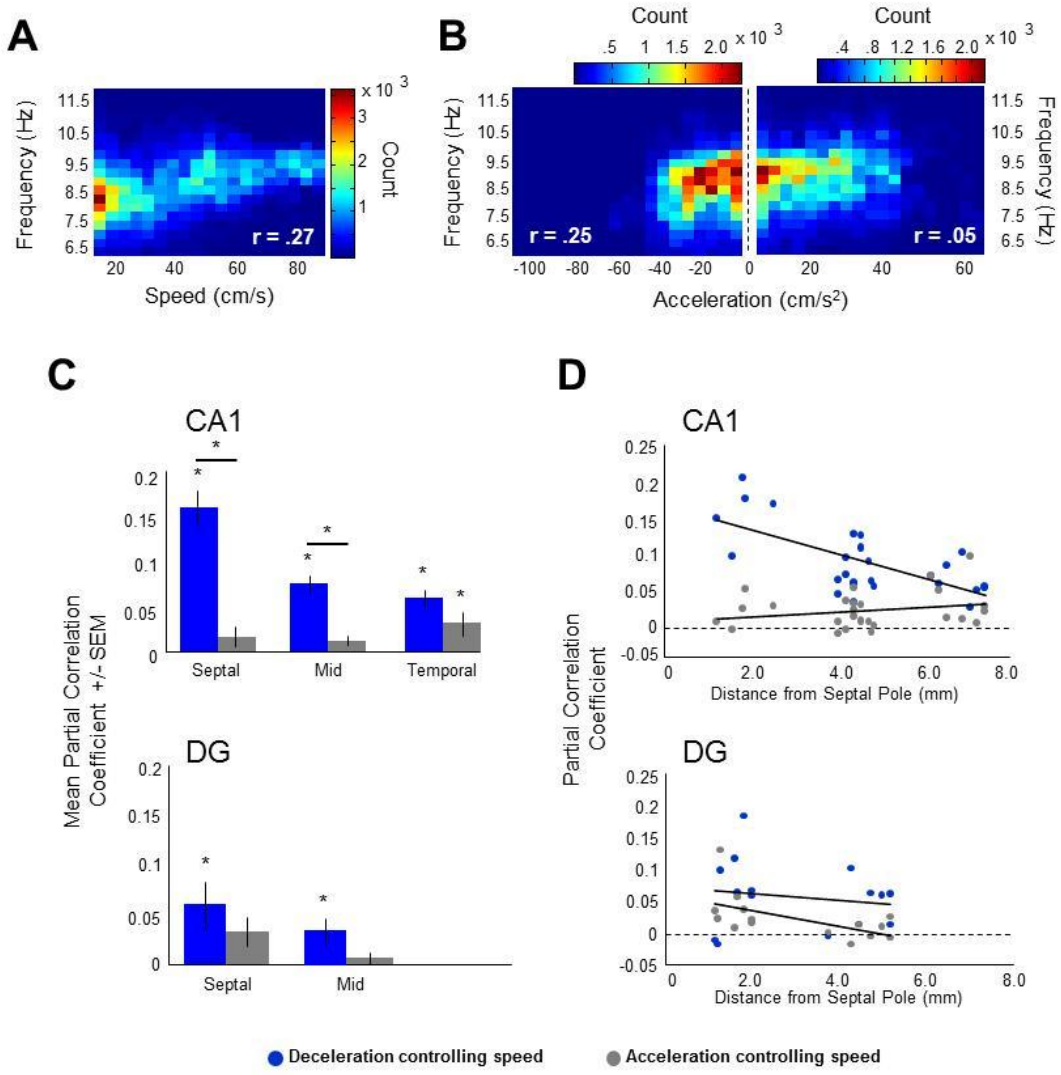
A
B
C
D
Frequency (Hz)
Speed (cm/s)
Count
r = .27
r = .25
r = .05
Acceleration (cm/s²)
CA1
DG
Septal
Mid
Temporal
Mean Partial Correlation Coefficient +/- SEM
Partial Correlation Coefficient
Distance from Septal Pole (mm)
Deceleration controlling speed
Acceleration controlling speed

Figure 7. *Relationship between acceleration, deceleration and theta frequency*. A *(left*): two-dimensional histograms of the relationship between speed and theta frequency for a representative septal CA1 electrode. B: same as left figure, but for all acceleration (deceleration, left; acceleration, right). C: All CA1 (top) and DG (bottom) electrodes were grouped according to septotemporal position in order to assess the relationship between acceleration, deceleration and theta frequency across the long axis of the hippocampus. The mean partial correlation coefficients for deceleration and theta frequency controlling for speed (blue bars) and acceleration and theta frequency controlling for speed (gray bars) across the longitudinal axis are shown. The relationship between acceleration and theta frequency was not negative, thus no rectification process was used. Theta frequency was significantly modulated by deceleration across the entirety of the hippocampus for both CA1 and DG sites, and only by acceleration in temporal extents of CA1 (*$P < 0.05$, t-test). Additionally, deceleration explained more of the variability in theta frequency across the entirety of the CA1 axis as compared to acceleration, with the exception of temporal CA1 (*$P < 0.05$, t-test). Furthermore, there was no difference in modulation of theta frequency by acceleration/deceleration across the septotemporal axis of DG (*$P > 0.05$, t-test). D: Partial correlation coefficients for the relationship between deceleration and theta frequency (blue circles) and acceleration and theta frequency (red circles) as a function of distance from the septal pole for CA1 (top) and DG (bottom). Each dot represents the partial correlation coefficient between each index (acceleration, deceleration) and theta frequency plotted as a function of distance from the septal pole. The relationship between deceleration and theta frequency decreased across the septotemporal axis of CA1 (*$P < 0.05$, correlation), but not DG (*$P > 0.05$, correlation), while the relationship between acceleration and theta frequency remained constant across the long axis of CA1 (*$P > 0.05$, correlation), but not DG (*$P < 0.05$, t-test, correlation).

Discussion

Alterations in ensemble activity as measured by LFP signals (power) are a useful tool to measure moment-by-moment dynamics across the areal axis of the HPC. Dynamic variation in these signals are highly related to online sensorimotor experience (speed, acceleration) and cognitive operations (Kay, 2005; Ulanovsky and Moss, 2007; Rizzuto et al., 2006; Montgomery et al., 2009; Tort et al., 2009; Shirvalkar et al., 2010). The advancement in the quantification of locomotor indices, such as speed and acceleration, should facilitate a better understanding of how these variables contribute to cognitive processing demands.

The present research demonstrates that acceleration, over and above the influence of speed, significantly contributes to explaining variability in theta amplitude. Most notable, we observed that when acceleration was divided into its positive and negative constituents, negative acceleration (deceleration) contributed most to explaining variability in theta amplitude (~16% in septal CA1), while positive acceleration (acceleration) had a relatively minimal contribution, in both DG and CA1 (~2% in septal CA1). Furthermore, the relationship between deceleration and theta amplitude decreased across the septotemporal axis of the HPC in CA1, but not in DG, while the relationship between acceleration and theta amplitude exhibited a somewhat opposite effect – it increased across the long axis of DG, but not CA1 (note that partial correlation coefficients presented on scatter plots have been rectified, thus the relationship between theta amplitude and acceleration actually increased across the long axis of DG, not decreased).

What's more, there exists a positive relationship between deceleration and theta frequency in both CA1 and DG, while theta frequency only slightly increased as a function of acceleration in temporal aspects of CA1. Theta frequency data is consistent with theta amplitude data, such that deceleration explains more variability in theta amplitude as compared to acceleration.

Our most straightforward finding is that acceleration (positive and negative taken together) predicts theta amplitude at septal CA1 and DG sites, and that this relationship decreases across the septotemporal axis of CA1, but not DG. More specifically, deceleration explains much more variability in theta amplitude relative to acceleration. To our knowledge, a systematic study examining the effect of whole body acceleration on theta indices has not been conducted until recently (Gupta et al., 2012; Molter et al., 2012; See Ledberg & Robbe 2011 with regards to head acceleration and theta oscillations), while others have noted its potential influence (Wyble et al., 2004; Sinnamon, 2000).

Where does the locomotor signal come from?

Given the prominent amount of variability in the theta signal that can be explained by whole body acceleration and locomotor speed, it is surprising that most studies do not control for locomotion-based variables when attempting to relate theta indices to cognitive operations (Montgomery et al., 2009). Furthermore, the evidence is unclear in regards to anatomic origination of this prominent speed and acceleration signal, despite its large effect on hippocampal

physiology. “Automatic” behaviors such as chewing, licking, etc are associated with irregular hippocampal activity where more “voluntary” movements such as walking, running, etc are associated with hippocampal theta activity (or rhythmic slow activity). Activation of RSA in the HPC is an indirect result of afferent input impinging upon the medial septum by means of brainstem input (Arnolds et al., 1977; Lee et al., 1994). Typically, increases in input strength are associated with increases in RSA frequency (Paiva et al, 1976) and at extremely high input strengths the relationship between medial septal input and increases in theta frequency is not faithfully transmitted (Arnolds et al., 1984). As posited by Arnolds et al., 1984, at high input strengths, frequency and amplitude become inversely related, such that at extremely high frequencies, amplitude decreases until a complete desynchronization occurs and becomes reminiscent of small irregular activity, as described by Vanderwolf et al., 1975.

With this idea in mind, locomotor inputs could modulate hippocampal theta activity by means of multiple sources. Medial thalamic areas are thought to be important for the initiation of voluntary movements, such as walking, running and avoidance behaviors (Vanderwolf, 1971). Furthermore, the vestibular system is implicated in stabilization of place cells (Russell et al., 2003) and spatial memory (Baek et al., 2010) where disruptions to the vestibular system produce decreases in theta indices (Smith et al., 2005). Moreover, proprioceptive, visual and motor information can indirectly reach the hippocampus through the medial septum and or entorhinal cortex (Smith et al., 2005). More than likely, speed and acceleration information reaches the hippocampus through the dynamic

interaction of multiple systems related to motor and sensory phenomena. Furthermore, given the knowledge that slower frequencies recruit larger pools of neurons (Sirota et al., 2008; Buzsaki et al., 2012), it is likely that the neural "topography" of voluntary movements (such as running), is highly complicated and integrated compared to that of automatic movements (Vanderwolf, 1969).

"Shunting" of theta amplitude as a function of high acceleration and deceleration can be supported in light of the sensorimotor integration hypothesis put forth by Bland & Oddie, 2001 and data from Wyble and colleagues, 2004. The sensorimotor integration hypothesis states that type 2 theta is generated by medial septal cholinergic mechanisms and functions to prepare the motor system for activity. If motor activity occurs, type 1 theta, or movement related theta ensues in combination with motor activity. With this idea in mind, Wyble and colleagues had rats shuttle between two ends of a track for a palatable food reward that was offered only at one end of the track. Their data demonstrate a sharp decrease in theta power 240-400 milliseconds before the cessation of motor activities only at the baited end of the track, while power at the non-baited end of the track remained relatively constant.

While the sensorimotor integration hypothesis focuses on the initiation of voluntary movement and its relation to theta indices, data presented here and by Wyble et al., 2004 suggest that, just as theta activity precedes commencement of motor activity, a shunting of theta power precedes activities not typically associated with theta (consummatory acts). When relating such an idea to the present data, sharp decreases in theta amplitude are observed with high levels of

acceleration (positive and negative), which are associated with the initiation of movement (high positive acceleration) and the cessation of movement (high negative acceleration). As supported by Wyble et al., 2004, theta amplitude drops relatively sharply during negative acceleration (deceleration) as compared to positive acceleration. These supporting data could explain why the relationship seen between negative acceleration and theta amplitude is much stronger than the relationship observed between positive acceleration and theta amplitude. Moreover, a clearer interpretation that supports the sensorimotor integration hypothesis is that changes in theta amplitude precede locomotor activity by hundreds of milliseconds.

The findings of the current research highlight the importance of controlling for locomotor indices when attempting to relate theta indices to cognitive operations (Vanderwolf, 1971). Experimental paradigms that require manipulations will most likely result in behavioral alterations (decreased running speed, sniffing, rearing, etc), which will constrain and subsequently alter theta spectral indices. With the knowledge that speed and acceleration contribute to explaining variability in theta amplitude, careful measures need to be taken in order to control for these highly quantifiable variables. Only then can conclusions be drawn about the relative influence of theta indices on cognitive processes.

Our laboratory is particularly interested in variation in theta dynamics across the septotemporal axis of the HPC and how its relationship to ongoing sensory processing as it relates to cognitive operations. In this vein, alterations in ensemble activity as measured by LFP signals are a useful tool to measure the

moment-to-moment variations in theta dynamics across the areal axis of the HPC. Dynamics in these signals are highly related to online sensorimotor process, cognitive operations and path integration (Whishaw & Maaswinkel, 1998; Buzsaki, 2005; Kay, 2005; McNaughton et al., 2006; Rizzuto et al., 2006; Ulanovsky and Moss, 2007; Montgomery et al., 2009; Tort et al., 2009; Shirvalkar et al., 2010). The present findings demonstrate a distributed and dynamic pattern of hippocampal theta LFPs with regards to whole body acceleration.

Chapter Three: Discussion

The present findings demonstrate that whole body acceleration significantly predicts theta amplitude, over and above the influence of locomotor speed. Most strikingly, when acceleration is divided into its positive and negative constituents, negative acceleration (deceleration) explained much more of the variability in theta amplitude as compared to positive acceleration (acceleration). More specifically, acceleration showed a slight negative relationship with theta amplitude (mean r-value = -.15 for all CA1 septal electrodes), while we observed a prominent positive relationship between deceleration and theta amplitude (mean r-value = .4 for all CA1 septal electrodes) in both CA1 and DG. Furthermore, the relationship between negative acceleration and theta amplitude decreased across the long axis of CA1, but not in DG, while the effect of positive acceleration remained constant across the long axis of CA1 and increased across the long axis of DG.

A possible explanation for the witnessed "shunting" of theta amplitude as a function of high accelerations (both positive and negative) can be supported in light of the sensorimotor integration hypothesis put forth by Bland & Oddie, 2001 and data from Wyble and colleagues, 2004. The sensorimotor integration hypothesis states that type 2 theta (atropine sensitive and associated with immobility) is generated by medial septal cholinergic mechanisms and functions to prepare the motor system for activity - a "readiness signal." If motor activity occurs, type 1 theta (atropine resistant, associated with locomotion) ensues in

combination with motor activity. With this idea in mind, Wyble and colleagues had rats shuttle between two ends of a track for a palatable food reward that was offered only at one end of the track. Their data demonstrate a sharp decrease in theta power 240-400 milliseconds before the cessation of motor activities only at the baited end of the track, while power at the non-baited end of the track remained relatively constant. Our data support this idea, as depicted in Figure 5.

While the sensorimotor integration hypothesis focuses on the initiation of voluntary movement and its relation to theta indices, data presented here and by Wyble et al., 2004 suggest that, just as theta activity precedes commencement of motor activity, a shunting of theta power precedes activities not typically associated with theta (consummatory acts). When relating such an idea to the present data, sharp decreases in theta amplitude are observed with high levels of acceleration (positive and negative), which are associated with the initiation of movement (high positive acceleration) and the cessation of movement (high negative acceleration). As supported by Wyble et al., 2004, theta amplitude drops relatively sharply during negative acceleration (deceleration) as compared to positive acceleration. These supporting data could explain why the relationship seen between negative acceleration and theta amplitude is much stronger than the relationship observed between positive acceleration and theta amplitude. Moreover, a clearer interpretation that supports the sensorimotor integration hypothesis is that changes in theta amplitude precede locomotor activity by hundreds of milliseconds.

Integration of multiple sensory systems

Anatomical studies suggest that regions of the thalamus could transfer vestibular information to the hippocampus via the parietal cortex (Smith, 1997; Save & Poucet, 2000 for reviews; Wiener et al., 2002). Given the knowledge that multiple sensory systems converge onto the vestibular nucleus complex (VNC) demonstrates the complex and extensive processing of vestibular information and integration with other sensory systems, even at brainstem levels. The associative parietal cortex (APC) could contribute to hippocampal function by initial integration of visuospatial information and self-motion information that is necessary for the combination of egocentrically acquired information into allocentrically coded information, which is performed by the hippocampus. The parietal cortex has monosynapic projections to vestibular brainstem nuclei (Guldin et al., 1992; 1993). Taken together, these findings suggest that the APC processes vestibular information as well as visual and somatosensory information.

Furthermore, the vestibular system is implicated in stabilization of place cells (Russell et al., 2003) and spatial memory (Smith et al., 2010). In the absence of reliable environmental cues (eg, darkness) cells maintain stable place fields (Sharp et al., 1995) suggesting that internal vestibular and tactile information could play a crucial role in generation a self-motion signal. Moreover, disruptions to the vestibular system produce decreases in theta indices (Russell et al., 2003). Additionally, proprioceptive, visual and motor information can indirectly reach the hippocampus through the medial septum and or entorhinal

cortex (Smith et al., 2005). More than likely, speed and acceleration information reaches the hippocampus through the dynamic interaction of multiple systems.

Theoretical suggestion

With present data in mind, theta amplitude appears to be more suggestive of future motor activities (or behavioral state) than of current conditions (Vanderwolf, 1969). This implication suggests more of a role for theta in the planning, coordination and maintenance of motor activity. While the "precession" of theta power in relation to motor activity has been described for the transition from a "non-theta" to a "theta" state (Vanderwolf, 1969), data here, as supported by Wyble et al., 2004, make the suggestion that this transition has the potential to occur in the opposite direction. Wyble and colleagues note that at the unrewarded end of the track rats stop walking but remain involved in exploratory sniffing behaviors. In opposition, at the rewarded end of the track rats engaged in consummatory acts (eg, eating) that is thought to be accompanied by large-amplitude irregular activity (Green & Arduini, 1954; Vanderwolf, 1969). In either case, theta dynamics appear to reflect the "behavioral state" of the animal hundreds of milliseconds preceding the behavior itself. Therefore, the behavioral context can largely affect the degree of theta expression (Lier et al., 2003).

Future Direction

Speed & acceleration modulation of theta indices across the proximodistal axis of septal CA1

CA1 principal cells receive direct input from space-tuned cells (grid cells) in medial entorhinal corex (MEC) as well as cells in lateral entorhinal cortex (LEC), which are thought to be more non-spatial in nature (Giocomo et al., 2007; Brun et al., 2008; Deshmukh et al., 2010; Henriksen et al., 2010). Proximal CA1, bordering CA3, receives prominent input from MEC, whereas distal CA1 bordering the subiculum, receives prominent input from LEC. With this idea in mind, Henriksen et al., 2010 asked the question if spatial tuning is graded along the proximodistal (or transverse) axis of septal CA1. In fact, distal CA1 cells showed less concise firing, had a larger number of firing fields and displayed less phase-locking of spikes to MEC theta oscillation compared to that of proximal CA1 cells. In the same vein as data shown here, an interesting question to address regarding spatial tuning across the proximodistal axis is the idea of speed and acceleration modulation of theta indices across the transverse axis of septal CA1. Further investigations regarding septotemporal variation in speed and acceleration modulation of theta amplitude across the proximodistal axis of CA1 will be more complicated to address because of the sharp increase in the angle of CA1 principal cells across the longitudinal axis. However, previous data support the role for functional differentiation across the septotemporal transverse axis of CA1.

Shifting speed, acceleration and theta signals in time

With the sensorimotor integration hypothesis in mind and the "precession" of theta activity in relation to locomotor indices, it seems viable that an experiment could be conducted where rats shuttle between ends of long linear track while speed, acceleration and position information are obtained. With access to these continuous signals, the signals could then be shifted in time in order to ascertain if theta amplitude is more related to past, present or future movement (speed and acceleration). Based on previous findings, it seems as though a shifting of the theta signal would be more related to future movements. Furthermore, we could vary the "integration window" and examine how this relationship changes (or doesn't change) across the septotemporal axis of the HPC. Given the knowledge that place cells increase in size across the septotemporal axis of the HPC (Jung et al., 1994) and temporal hippocampus is thought to code for more allocentrically-tuned information, a logical hypothesis would suggest that the integration window across the septotemporal axis would widen.

Controlling for locomotor indices allows for the relation of theta to cognition during a cued auditory task

The findings of the current research highlight the importance of controlling for locomotor indices when attempting to relate theta indices to cognitive operations (Vanderwolf, 1971). Experimental manipulations will most likely result in behavioral alterations (decreased running speed, sniffing, rearing, etc), which

will constrain theta spectral indices. With the knowledge that speed and acceleration contribute to explaining variability in theta amplitude, careful measures need to be taken in order to control for these highly quantifiable variables. With this idea in mind, only then can conclusions be drawn about the relative influence of theta indices on cognitive processes. Because our lab is aware of the contribution of these locomotor indices and is proficient at controlling for them, the next step would be to have a locomotor task that includes a higher cognitive load than shuttling between two ends of a linear track.

Recently, the suggestion has been made that speed has lower predictability power in explaining theta indices when cognitive variables are present (Montgomery et al., 2009). A memory task could be employed with varying cognitive load to probe this issue. Rats can be trained to perform a delayed match (or non-match) to place task on a modified T-maze (Figure 8A).

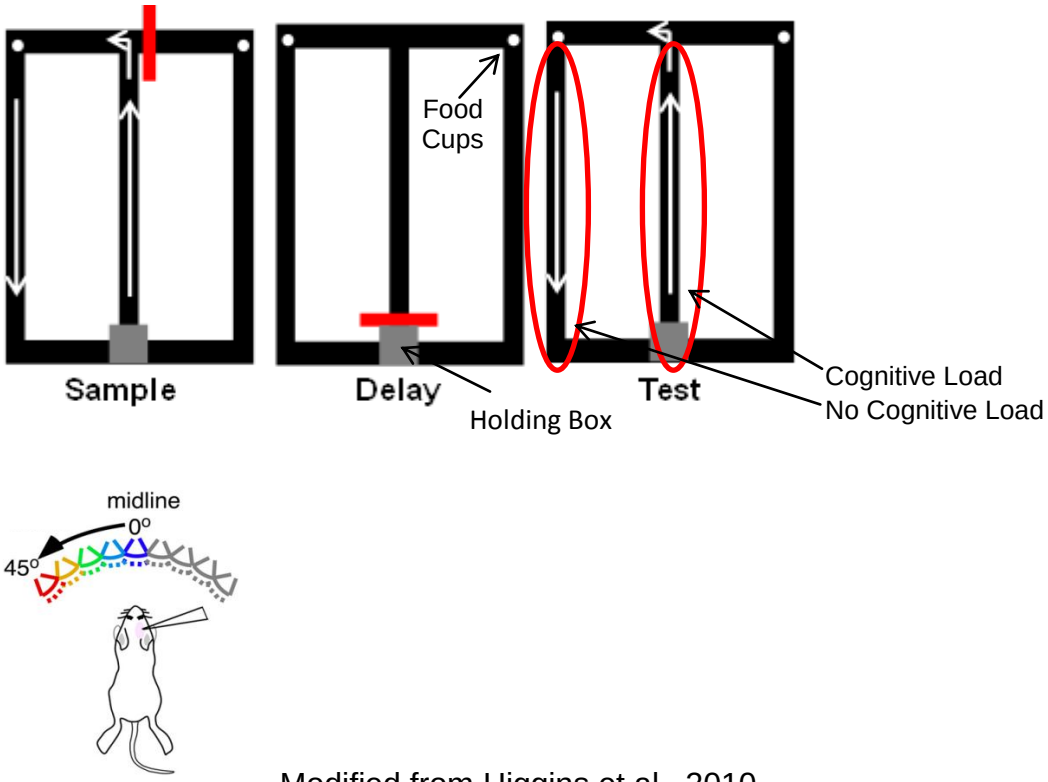

Modified from Higgins et al., 2010

Figure 8. *Delayed match to sample modified T-maze paradigm and cognitive load*. **A**: Trained rats will traverse a match to sample T-maze for food reward (while cups). Rats will be released from the holding box and given a sample trial in which they have to remember the location of a food reward. In order to vary cognitive load, the animals can experience delays of varying lengths in the holding box, or can be presented with tones of varying degrees from the midline (**B**). Traversals in the center stem represent trials in which a cognitive load of varying degrees is present, while traversals on the outside of the maze represent trials that lack cognitive load. These traversals can be directly compared in order to parse out the role of cognition to theta indices while controlling for locomotor activities.

In order to vary the cognitive load of the task, the presence of a tone, the sequence of tones presented, the relationship of a tone from the midline (Figure 8B), or the amount of time in the holding box could be manipulated. If the animal makes a correct choice, he will be rewarded (Figure 8A, white circles indicate reward cups), if the animal fails to make a correct choice, no reward will be given. The center stem represents the choice trial, with varying difficulties, while the outside stems represent the return trials (to the holding box), which presumably lack cognitive operations. These two stems (cognitive vs not-cognitive) could be compared in order to measure the relative contribution of locomotor activities to theta indicies while cognitive variables are present.

Final Conclusion

Alterations in ensemble activity as measured by LFP signals are a useful tool to measure the moment-to-moment variations in theta dynamics across the areal axis of the HPC. Dynamics in these signals are highly related to online sensorimotor process, cognitive operations and path integration (Whishaw, 1998; Buzsaki, 2005; Kay, 2005; McNaughton et al., 2006; Rizzuto et al., 2006; Ulanovsky and Moss, 2007; Montgomery et al., 2009; Tort et al., 2009; Shirvalkar et al., 2010). While LFP measurements, such as theta, coordinate the timing of action potential discharge, the theta signal carries more information than what has previously been thought. Although a clocking mechanism, information can be extracted from the theta signal that predicts ongoing sensorimotor experience

("phase precession", O'Keefe & Recce, 1993) and proves to be a more sensitive measure than what previous research might suggest. Changes in firing rates of hippocampal principal cells as a function of environment (Royer et al., 2010), reward contingency (Wyble et al., 2004; Chrobak Lab, unpublished observations), and novelty (Fyhn et al., 2002; Jeewajee et al., 2008) have the potential to be reflected in the large-scale network dynamics of the LFP (Penley et al., 2011; Chrobak Lab, unpublished observations) In this vein, LFP measurements are a useful index for hippocampal function.

References

Ahmed OJ, Mehta MR (2012) Running speed alters the frequency of hippocampal gamma oscillations *J Neurosci* 21(32): 7373-83).

Alonso A, Garcia-Austt (1987) Neuronal sources of theta rhythm in the entorhinal cortex of the rat. I. Laminar Distribution of theta field potentials. *Exp Brain Res* 67: 493-501.

Amaral DG, Kurz J (1985) An analysis of the origins of the cholinergic and noncholinergic septal projections to the hippocampal formation of the rat. *J Comp Neurol* 240: 37-59.

Amaral DG, Witter, MP (1989) The three-dimensional organization of the hippocampal formation: a review of anatomical data. *Neuroscience* 31:371-391.

Ang CW, Carlson GC, Coulter DA (2005) Hippocampal CA1 circuitry dynamically gates direct cortical inputs preferentially at theta frequencies. *J Neurosci* 42:9567-9580.

Anderson P, Bliss TV, Skrede KK (1971) Lamellar organization of hippocampal pathways. *Exp Brain Res* 2:222-238.

Arnolds DEAT, Lopes da Silva FH, Aitink JW, Kamp A (1977) Motor acts and firing of reticular neurons correlated with operantly reinforced hippocampus theta shifts. *Brain Res* 85:194-195.

Arnolds DE, Lopes da Silva RH, Boeijinga P, Kamp A, Aitink W (1984) Hippocampal EEG and motor activity in the cat: the role of eye movements and body acceleration. *Behav Brain Res* 12: 121-35.

Asaka Y, Mauldin KN, Griffin AL, Seager MA, Shurell E, Berry SD (2005) Nonpharmacological amelioration of age-related learning deficits: the impact of hippocampal theta-triggered training. *PNAS* 102:13284-13288.

Baek JH, Zheng Y, Darlington CL, Smith PF (2010) Evidence that spatial memory deficits following bilateral vestibular deafferentation in rats are probably permanent. *Neurobiol Learn Mem* 94:402-413.

Baisden RH, Woodruff ML, Hoover DB (1984) Cholinergic and non-cholinergic septo-hippocampal projections: a double-label horseradish peroxidase-acetylcholinesterase study in the rabbit. *Brain Research* 290:146-151.

Bannerman DM, Rawlins JN, McHugh SB, Deacon RM, Yee BK, Bast T, Zhang WN, Pothuizen HH, Feldon J (2004) Regional dissociations within the hippocampus--memory and anxiety. *Neurosci Biobehav Rev* 28:273-283.

Bernardo LS, Prince DA (1982) Cholinergic excitation of mammalian hippocampal pyramidal cells. *Brain Res* 249:315-331.

Berry SD, Rinaldi PC, Thompson RF, Verzeano M (1978) Analysis of temporal relations among units and slow waves in rabbit hippocampus. *Brain Res Bull* 3:509-18.

Bjarkam CR, Sorensen JC, Geneser FA (2003) Distribution and morphology of serotonin-immunoreactive axons in the hippocampal region of the New Zealand while rabbit. I. area dentate and hippocampus. *Hippocampus* 13:21-37.

Bland BH (1986) Physiology and pharmacology of hippocampal formation theta rhythms. *Prog in Neurobiology* 26:1-54.

Bland BH, Jackson J, Derrie-Gillespie D, Azad T, Richhi A, Abriam J (2006) Amplitude, frequency, and phase analysis of hippocampal theta during sensorimotor processing in a jump avoidance task. *Hippocampus* 16:673-681.

Bland BH, Oddie SD (2001) Theta band oscillation and synchrony in the hippocampal formation and associated structures: the case for its role in sensorimotor integration. *Behav Brain Res* 127:119-36.

Borhegyi ZM, Acsady L, Freund TF (1997) The supramammillary nucleus innervates cholinergic and GABAergic neurons in the medial septum-diagonal band of broca complex. *Neurosci* 82:1053-1065.

Borhegyi ZM, Varga V, Szilagyi N, Fado D, Freund TF (2004) Phase segregation of medial septal GABAergic neurons during hippocampal theta activity. *J Neurosci* 24:8470-9.

Bouwman BM, van Lier H, Nitert HE, Drinkenburg WH, Coenen AM, van Rijn CM (2005) The relationship between hippocampal EEG theta activity and locomotor behavior in freely moving rats: effects of vigabatrin. *Brain Res Bull* 64: 505-9.

Bragin A, Jando G, Nadasdy Z, Hetke J, Wise K, Buzsaki G (1995) Gamma (40-100 Hz) oscillation in the hippocampus of the behaving rat. *J Neurosci* 15:47-60.

Brankack AJ, Stewart M, Fox SE (1993) Current source density analysis of the hippocampal theta rhythm: associated sustained potentials and candidate synaptic generators. *Brain Res* 615:310-327.

Brazhnik ES, Fox SE (1997) Intracellular recordings from medial septal neurons during hippocampal theta rhythm. *Exp Brain Res* 114:442-453.

Brazhnik ES, Fox SE (1999) Action potentials and relations to the theta rhythm of medial septal neurons in vivo. *Exp Brain Res* 127: 244-58.

Brun VH, Solstad T, Kjelstrup KB, Fyhn M, Witter MP, Moser EI, Moser MB (2008) Progressive increase in grid scale from dorsal to ventral medial entorhinal cortex. *Hippocampus* 18:1200-1212.

Buzsaki G (1989) Two-stage model of memory trace formation: A role for “noisy” brain states. *Neurosci* 31:551-570.

Buzsaki G, Chrobak JJ (1995) Temporal structure in spatially organizaed neuronal ensembles: a role for interneuronal networks. *Curr Opin Neurobiol* 5:504-510.

Buzsaki G (2002) Theta oscillations in the hippocampus. *Neuron* 33:325-340.

Buzsaki G (2005) Theta rhythm of navigation: link between path integration and landmark navigation, episodic and semantic memory. *Hippocampus* 15:827-40.

Buzsaki G, Anastassiou CA, Koch C (2012) The origin of extracellular fields and currents – EEG, ECoG, LFP and spikes. *Nat Neurosci Rev* 13:407-420.

Burgess N, Maguire EA, O’Keefe J (2002) The human hippocampus and spatial and episodic memory. *Neuron* 35: 625-41.

Burwell, RD (2000) The parahippocampal region: corticocortical connectivity. *Annals NY Acad Sci* 401:25-42.

Canolty RT, Edwards E, Dalal SS, Soltani M, Nagarajan SS, Kirsch HE, Berger MS, Barbaro NM, Knight RT (2006) High gamma power is phase-locked to theta oscillations in human neocortex. *Science* 313: 1626-8.

Chrobak JJ, Amaral DG (2007) Entorhinal cortex of the monkey: VII. Intrinsic connections. *J Comp Neurol* 500: 612-33.

Chrobak JJ, Buzsaki G (1994) Selective activation of deep layer (V-VI) retrohippocampal cortical neurons during hippocampal sharp waves in the behaving rat. *J Neurosci* 14:6160-70.

Chrobak JJ, Buzsaki G (1998) Operational dynamics in the hippocampal-entorhinal axis. *Neurosci & Biobehav Rev* 22:303-10.

Colom LV, Castaneda MT, Reyna T, Hernandez S, Garrido-Sanabria E (2005) Characterization of medial septal glutamatergic neurons and their projection to the hippocampus. *Synapse* 58:151-64.

Conrad LCA, Leonard DWP (1974) Connections of the median and dorsal raphe nuclei in the rat: an autoradiographic and degeneration study. *J Comp Neurol* 156:179-205.

Deshmukh SS, Yoganarasimha D, Voicu H, Knierim JJ (2010) Theta modulation in the medial and the lateral entorhinal cortices. *J Neurophysiol* 104:994-1006.

Dolleman-Van der Weel MJ, Witter MP (2000) Nucleus reuniens thalami innervates y aminobutyric acid positive cells in hippocampal field CA1 of the rat. *Neurosci Letters* 278:145-148.

Dolorfo C, Amaral DG (1998a) Entorhinal cortex of the rat: Topographic organization of the cells of origin of the perforant path projections to the dentate gyrus. *J Comp Neurol* 398:25-48.

Dolorfo CL, Amaral DG (1998b) Entorhinal cortex of the rat: organization of intrinsic connections. *J Comp Neurol* 398:49-82.

Dragoi G, Buzsaki G (2006) Temporal encoding of place sequences by hippocampal assemblies. *Neuron* 50:145-157.

Ekstrom A, Caplan E, Ho E, Shattuck K, Fried I, Kahana MJ (2005) Human hippocampal theta activity during virtual navigation. *Hippocampus* 15:881-89.

Fano S, Caliskan G, Behrens CJ, Heinemann U (2011) Histaminergic modulation of acetylcholine-induced theta oscillations in rat hippocampus. *Neuroreport* 22:520-24.

Feder R, Ranck JB Jr (1973) Studies on single neurons in dorsal hippocampal formation and septum of unrestrained rats. II. Hippocampal slow waves and theta cell firing during bar pressing and other behaviors. *Exp Neurol* 41: 532-55.

Fell J, Klaver P, Lehnertz K, Grunwald T, Schaller C, Elger CE, Fernandez G. (2001) Human memory formation is accompanied by rhinal-hippocampal coupling and decoupling. *Nat Neurosci*. Dec;4(12):1259-64.

Freund TF, Antal M (1988) GABA-containing neurons in the septum control inhibitory interneurons in the hippocampus. *Nature* 336:170-173.

Fyhn M, Molden S, Hollup S, Moser MB, Moser EI (2002) Hippocampal neurons responding to first-time dislocation of a target object. *Neuron* 35:555-566.

Gage FH, Thompson RG (1980) Differential distribution of norepinephrine and serotonin along the dorsal-ventral axis of the hippocampal formation. *Brain Res Bull* 5: 771-3.

Gaykema RPA, Luiten PGM, Nyakas C, Traber J (1990) Cortical projection patterns of the medial septum-diagonal band complex. *J Comp Neurol* 124:103-124.

Giocomo LM, Zilli EA, Fransen E, Hasselmo ME (2007) Temporal frequency of subthreshold oscillations scales with entorhinal grid cell field spacing. *Science* 315:1719-1722.

Gray CM (1994) Synchronous oscillations in neuronal systems: mechanism and functions. *J Comp Neurosci* 1:11-38.

Green JD, Arduini AA (1954) Hippocampal electrical activity in arousal. *J Neurophysiol* 17: 533-57.

Guldin WO, Akbarian S, Grusser OJ (1992) Cortico-cortical connections and cytoarchitectonics of the primate vestibular cortex: a study in squirrel monkeys (*Saimiri sciureus*). *J Comp Neurol* 326:375-401.

Guldin WO, Mirring S, Grusser OJ (1993) Connections form the neocortex to the vestibular brain stem nuclei in the common marmoset. *Neuroreport* 2:113-116.

Gusev PA, Cui C, Alkon DL, Gubin AN (2005) Topography of Arc/Arg3.1 mRNA expression in the dorsal and ventral hippocampus induced by recent and remote spatial memory recall: dissociation of CA3 and CA1 activation. *J Neurosci* 25:9384-9397.

Gupta AS, van der Meer, MA, Touretzky DS, Redish AD (2012) Segmentation of spatial experience by hippocampal theta sequences. *Nat Neurosci* 15:1032-1039.

Hajos N, Palhalmi J, Mann EO, Nemeth B, Paulsen O, Freund TF (2004) Spike timing of distinct types of GABAergic interneurons during hippocampal gamma oscillations in vitro. *J Neurosci* 24: 9127-37. *Europ J Neurosci* 4:144-153.

Halasy K, Miettinen R, Szabat E, Freund TF (1992) GABAergic interneurons are the major postsynaptic targets of median raphe afferents in the rat dentate gyrus.

Haring JH, Davis JN (1985) Differential distribution of locus coeruleus projections to the hippocampal formation: anatomical and biochemical evidence. *Brain Res* 325:366-369.

Harris KD, Csicsvari J, Hirase H, Dragoi G, Buzsaki G (2003) Organization of cell assemblies in the hippocampus. *Letters to Nature* 424:552-556.

Hasselmo ME, Bodelon C, Wyble BP (2002) A proposed function for hippocampal theta rhythm: separate phases of encoding and retrieval enhance reversal of prior learning. *Neural Computation* 14:793-817.

Hasselmo ME (2005) What is the function of hippocampal theta rhythm? – linking behavioral data to phasic properties of field potential and unit recording data. *Hippocampus* 15:936-49.

Henriksen EJ, Colgin LL, Barnes CA, Witter MP, Moser MB, Moser EI (2010) Spatial representation along the proximodistal axis of CA1. *Neuron* 68:127-137.

Henze DA, Urban NN, Barrionuevo G (2000) The multifarious hippocampal mossy fiber pathway: a review. *Neurosci* 98:407-427.

Herkenham M (1978) The connections of the nucleus reuniens thalami: evidence for a direct thalamo-hippocampal pathway in the rat. *J Comp Neurol* 177:589-609.

Higgins NC, Storace DA, Escabi MA, Read HL (2010) Specialization of binaural responses in ventral auditory cortices. *J Neurosci* 30:14522-14532.

Hinman JH, Penley SC, Long LL, Escabi MA, Chrobak JJ (2011) Septotemporal variation in dynamics of theta: speed and habituation. *J Neurophysiol* 105:2645-2686.

Jeewajee A, Lever C, Burton S, O'Keefe J, Burgess N (2008) Environmental novelty is signaled by reduction of the hippocampal theta frequency. *Hippocampus* 18: 340-8.

Jung MW, Wiener SI, McNaughton BL (1994) Comparison of spatial firing characteristics of units in dorsal and ventral hippocampus of the rat. *J Neurosci* 14: 7347-56.

Jutras MJ, Fries P, Buffalo EA (2010) Gamma-band synchronization in the macaque hippocampus and memory formation. *J Neurosci* 29: 12521-31.

Kahana MJ, Sekuler R, Caplan JB, Kirschen M, Madsen JR (1999) Human theta oscillations exhibit task dependence during virtual maze navigation *Nature* 399:781-84.

Kahana MJ, Seelig D, Madsen JR (2001) Theta returns. *Curr Opin Neurobiol.* 11:739-744.

Kay LM (2005) Theta oscillations and sensorimotor performance. *Proc Natl Acad Sci* 102:3863-8.

King C, Recce M, O'Keefe J (1998) The rhythmicity of cells of the medial septum/diagonal band of Broca in the awake freely moving rat: relationship with behavior and hippocampal theta. *Eur J Neurosci* 10: 464-77.

Kjelstrup KB, Solstad T, Brun VH, Hafting T, Leutgeb S, Witter MP, Moser EI, Moser MB (2008) Finite scale of spatial representation in the hippocampus. *Science* 321: 140-3.

Kirk, IJ (1996) Evidence for differential control of posterior hypothalamic, supramammillary, and medial mammillary theta-related cellular discharge by ascending and descending pathways. *J Neurosci* 16:5547-5554.

Kirk IJ, Frequency modulation of hippocampal theta by the supramammillary nucleus, and other hypothalamic-hippocampal interactions: mechanisms and functional implications. (1998) *Neurosci & Biobehav Rev* 22:291-302.

Kiss J, Csaki A, Bokor H, Shanabrough M, Leranth C (2000) The Supramammillo-hippocampal and supramammillo-septal glutamatergic/aspartatergic projections in the rat: a combined [^{3}H]D-asparate autoradiographic and immunohistochemical study. *Neuroscience* 97:657-669.

Knake S, Wang CM, Ulbert I, Schomer DL, Halgren E (2007) Specific increase of human entorhinal population synaptic and neuronal activity during retrieval. *Neuroimage* 37:618-22.

Kocsis B, Vertes RP (1994) Characterization of neurons of the supramammillary nucleus and mammilary body that discharge rhythmically with the hippocampal theta rhythm in the rat. *J Neurosci* 14:7040-7052.

Kocsis B, Bragin A, Buzsaki G (1999) Interdependence of multiple theta generators in the hippocampus: a partial coherence analysis. *J Neurosci* 19:6200-6212.

Kohler C, Steinbusch H (1982) Identification of serotonin and non-serotonin-containing neurons of the mid-brain raphe projecting to the entorhinal area and the hippocampal formation. A combined immunohistochemical and

fluorescent retrograde tracing study in the rat brain. *Neurosci* 4:951-975.

Konopacki J, Bland BH, Colom LV, Oddie SD (1992) In vivo intracellular correlates of hippocampal formation theta-on and theta-off cells. *Brain Res* 586:247-55.

Lavenex P, Amaral DG (2000) Hippocampal-neocortical interaction: a hierarchy of associativity. *Hippocampus* 10:420-430.

Lavenex P, Amaral DG (2006) Hippocampal neuroanatomy. *The Hippocampus Book*, Oxford University Press. Ch 3.

Lorch RF Jr, Myers JL (1990) Regression analyses of repeated measures data in cognitive research. *J Exp Psychol Learn Mem Cogn* 16: 149-57.

Ledberg A, Robbe D (2011) Locomotion-related oscillatory body movements at 6–12 Hz modulate the hippocampal theta rhythm. *PLoS ONE* 11:27575.

Lee MG, Chrobak JJ, Sik A, Wiley RG, Buzsaki G. (1994) Hippocampal theta activity following selective lesion of the septal cholinergic system. *Neuroscience* 62: 1033-47.

Leung LS (1984) Pharmacology of theta phase shift in the hippocampal CA1 region of freely moving rats. *Electroencephalogr Clin Neurophysiol* 58: 457-66.

Leung L-WS (1985) Spectral analysis of hippocampal EEG in the freely moving rat: effects of centrally active drugs and relations to evoked potentials. *Electroencephalogr Clin Neurophysiol* 60:65-77.

Lier HV, Coenen AML, Drinkenburg WHIM (2003) Behavioral transitions modulate hippocampal electroencephalogram correlates of open field behavior in the rat: support for a sensorimotor function of hippocampal rhythmical synchronous activity. *J Neurosci* 23:2459-2465.

Lisman JE, Idiart MA (1995) Storage of 7 +/- 2 sort-term memories in oscillatory subcycles. *Science* 267: 1512-5.

Lisman J (2005) The theta/gamma discrete phase code occurring during the hippocampal phase precession may be a more general brain coding

scheme. *Hippocampus* 15:913-922.

Llinas RR, Grace AA, Yarom Y (1991) In vitro neurons in mammalian cortical layer 4 exhibit intrinsic oscillatory activity in the 10-50 Hz frequency range. *PNAS* 88:897-901.

Loughlin SE, Foote SL, Bloon FE (1986) Efferent projections of nucleus locus coeruleus: topographic organization of cells of origin demonstrated by three-dimensional reconstruction. *Neurosci* 18:291-306.

Loy R, Koziell DA, Lindsey JD, Moore RY (1980) Noradrenergic innervations of the adult rat hippocampal formation. *J Comp Neurol* 189: 699-710.

Lubenov EV, Siapas AG (2009) Hippocampal theta oscillations are travelling waves. *Nature* 459:534-539.

Lubke J, Deller T, Frotscher M (1997) Septal innervation of mossy cells in the hilus of the rat dentate gyrus: an anterograde tracing and intracellular labeling study. *Exp Brain Res.* 114:423-432.

Maggio N, Segal M (2007) Striking variations in corticosteroid modulation of long-term potentiation along the septotemporal axis of the hippocampus. *J Neurosci* 27:5757-5765.

Manseau F, Goutagny R, Danik M, Williams S (2008) The hippocamposeptal pathway generates rhythmic firing of GABAergic neurons in the medial septum and diagonal bands: an investigation using a complete septohippocampal preparation in vitro. *J Neurosci* 28:4096-107.

Maurer AP, Cowen SL, Burke SN, Barnes CA, McNaughton BL (2005) Self-motion and the origin of differential spatial scaling along the septo-temporal axis of the hippocampus. *Hippocampus* 15: 841-52.

McFarland WL, Teitelbaum H, Hedges EK (1975) Relationship between hippocampal theta activity and running speed in the rat. *J Comp Physiol Psychol* 88: 324-8.

McMahon LL, Kauer JA (1997) Hippocampal interneurons are excited via serotonin-gated ion channels. *J Neurophysiol* 78:2493-2502.

McNaughton N, Logan B, Panickar KS, Kirk IJ, Pan WX, Brown NT, Heenan A (1995) Contribution of synapses in the medial supramammillary nucleus to the frequency of hippocampal theta rhythm in freely moving rats. *Hippocampus* 5:534-545.

McNaughton BL, Battaglia FP, Jensen O, Moser EI, Moser MB (2006) Path integration and the neural basis of the 'cognitive map'. *Nat Neurosci Rev* 7 :663-678.

Molter C, O'Neil J, Yamaguchi Y, Hirase J, Leinekugel X (2012) Rhythmic modulation of theta oscillations supports encoding of spatial and behavioral information in the rat hippocampus. *Neuron* 75:889-903.

Moore RY, Halaris AE (2004) Hippocampal innervations by serotonin neurons of the midbrain raphe in the rat. *J Comp Neurol* 164:171-183.

Moser MB, Moser EI, Forrest E, Andersen P, Morris RG (1995) Spatial learning with a minislab in the dorsal hippocampus. *Proc Natl Acad Sci USA* 92:9697-9701.

Mosko S, Lynch G, Cotman CW (1973) The distribution of septal projections to the hippocampus of the rat. *J Comp Neurol*. 152: 163-174.

Montgomery SM, Betancur MI, Buzsaki G (2009) Behavior-dependent coordination of multiple theta dipoles in the hippocampus. *J Neurosci* 29:1381-94.

Nyakas C, Luiten PGM, Spencer DG, Traber J (1987) Detailed projection patterns of septal and diagonal band efferents to the hippocampus in the rat with emphasis on innervation of CA1 and dentate gyrus. *Brain Res Bull* 18:533-545.

Nyhus E, Curran T (2010) Functional role of gamma and theta oscillations in episodic memory. *Neurosci Biobehav* Rev 34: 1023-35.

O'Keefe J, Dostrovsky J (1971) The hippocampus as a spatial map. Preliminary evidence from unit activity in the freely-moving rat. *Brain Res* 34: 171-5.

Oleskevich S, Descarries L (1990) Quantified distribution of serotonin innervations in adult rat hippocampus. *Neuroscience* 34: 19-33.

Paiva T, Lopes da Silva FH, Mollevanger W (1976) Modulating systems of hippocampal EEG. *Electroenceph Clin Neurophysiol* 40:470-480.

Pan WX, McNaughton N (2004) The supramammillary area: its organization, functions and relationship to the hippocampus. *Prog Neurobiol* 74:127-66.

Panula P, Pirvola U, Auvinen S, Airaksinen MS (1989) Histamine-immunoreactive nerve fibers in the rat brain. *Neuroscience* 28: 585-610.

Patel J, Fujisawa S, Antal B, Royer S, Buzsaki G (2012) Traveling theta waves along the entire septotemporal axis of the hippocampus. *Neuron* 75:410-417.

Penley SC, Hinman JR, Sabolek HR, Escabi MA, Markus EJ, Chrobak JJ (2011) Theta and gamma coherence across the septotemporal axis during distinct behavioral states. *Hippocampus* 22:1164-1175.

Petsche H, Stumpf C, Gogolak G (1962) The significance of the rabbit's septum as a relay station between the midbrain and the hippocampus. I. The control of the hippocampus arousal activity by the septum cells. *Electroencephalogr Clin Neurophysiol* 14: 202-11.

Pickel VM, Segal M, Bloom FE (1974) A radioautographic study of the efferent pathways of the nucleus locus coeruleus. *J Comp Neurol* 155:15-41.

Pikkarainen M, Ronkko S, Savander V, Insausti R, Pitkanen A (1999) Projections from the lateral, basal, and accessory basal nuclei of the amygdale to the hippocampal formation in rat. *J Comp Neurol* 403: 229-60.

Pitkanen A, Pikkarainen M, Nurminen N, Ylinen A (2000) Reciprocal connections between the amygdala and the hippocampal formation, perirhinal cortex and postrhinal cortex in rat. A review. *Ann NY Acad Sci* 911:369-391.

Pitler TA, Alger BE (1992) Cholinergic excitation of GABAergic interneurons in the rat hippocampal slice. *J Physiol* 450:127-142.

Rivas J, Gaztelu JM, Garcia-Austt E (1996) Changes in hippocampal cell discharge patterns and theta rhythm spectral properties as a function of walking velocity in the guinea pig. *Exp Brain Res* 108: 113-8.

Rizzuto DS, Madsen JR, Bromfield EB, Schulze-Bonhage A, Kahana MJ (2006) Human neocortical oscillations theta phase differences between encoding and retrieval. *Neuroimage* 31:1352-1358.

Royer S, Sirota A, Patel J, Buzsaki G (2010) Distinct representations and theta dynamics in dorsal and ventral hippocampus. *J Neurosci* 30:1777-87.

Russell NA, Horii A, Smith PF, Darlington CL, Bilkey DK (2003) Long-term effects of permanent vestibular lesions on hippocampal spatial firing. *J Neurosci* 16:6490-6498.

Sabolek HR, Penley SC, Hinman JR, Bunce JG, Markus EJ, Escabi M, Chrobak JJ (2009) Theta and gamma coherence along the septotemporal axis of the hippocampus. *J Neurophysiol* 101:1192-200.

Save E, Poucet B (2000) Hippocampal-parietal cortical interactions in spatial cognition. *Hippocampus* 10:491-499.

Sederberg PB, Kahana MJ, Howard MW, Donner EJ, Madsen JR (2003) Theta and gamma oscillations during encoding predict subsequent recall. *J Neurosci* 23: 10809-14.

Sharp PE, Turner-Williams S (2005) Movement-related correlates of single-cell activity in the medial mammillary nucleus of the rat during a pellet-chasing task. *J Neurophysiol* 94:1920-1927.

Shin J, Talnov A (2001) A single trial analysis of hippocampal theta frequency during nonsteady wheel running in rats. *Brain Res* 897: 217-21.

Sinnamon HM (2000) Priming pattern determines the correlation between hippocampal theta activity and locomotor stepping elicited by stimulation in anesthetized rats. *Neurosci* 98:459-470.

Sinnamon HM (2006) Decline in hippocampal theta activity during cessation of locomotor approach sequences: amplitude leads frequency and relates to instrumental behavior. *Neuroscience* 140:779-790.

Sirota A, Montgomery S, Fujisawa S, Isomura Y, Zugaro M, Buzsaki G (2008) Entrainment of neocortical neurons and gamma oscillations by the hippocampal theta rhythm. *Neuron* 60:683-697.

Shirvalkar PR, Rapp PR, Shapiro ML (2010) Bidirectional changes to hippocampal theta-gamma comodulation predict memory for recent spatial episodes. *Proc Natl Acad Sci USA* 107:7054-7059.

Slawinska U, Kasicki S (1998) The frequency of rat's hippocampal theta rhythm is related to the speed of locomotion. *Brain Res* 796: 327-31.

Smith PF (1997) Vestibular-hippocampal interaction. *Hippocampus* 7:465-471.

Smith PF, Horii A, Russell N, Bilkey DK, Zheng Y, Liu P, Kerr DS, Darlington CL (2005) The effects of vestibular lesions on hippocampal function in rats. *Prog Neurobiol* 75:391-405.

Smith PF, Darlington CL, Zheng Y (2010) Move it or lose it – is stimulation of the vestibular system necessary for normal spatial memory? *Hippocampus* 20:36-43.

Snyder JS, Radik R, Wojtowicz JM, Cameron HA (2009) Anatomical gradients of adult neurogenesis and activity: young neurons in the ventral dentate gyrus are activated by water maze training. *Hippocampus* 19:360-370.

Strange BA, Fletcher PC, Henson RN, Friston KJ, Dolan RJ (1999) Segregating the functions of human hippocampus. *Proc Natl Acad Sci USA* 96:4034-4039.

Swanson LW, Wyss JM, Cowan WM (1978) An autoradiographic study of the organization of intrahippocampal association pathways in the rat. *J Comp Neurol* 181:681-715.

Swanson LW, Hartman BK (1975) The central adrenergic system. An immunofluorescence study of the location of cell bodies and their efferent connections in the rat utilizing dopamine-B-hydroxylase as a marker. *J Comp Neurol* 163:467-505.

Teitelbaum H, McFarland WL (1971) Power spectral shifts in hippocampal EEG associated with conditioned locomotion in the rat. *Physiolo Behav* 7: 545-9.

Thompson CL, Pathak SD, Jeromin A, Ng LL, MacPherson CR, Mortrud MT, Cusick A, Riley ZL, Sunkin SM, Bernard A, Puchalski RB, Gage FH, Jones AR, Bajic VB, Hawrylycz MJ, Lein ES (2008) Genomic anatomy of the

hippocampus. *Neuron* 60: 1010-21.

Tort AB, Komorowski RW, Manns JR, Kopell NJ, Eichenbaum H (2009) Theta-gamma coupling increases during the learning of item-context associations. *Proc Natl Acad Sci USA* 106: 20942–20947.

Toth K, Borhegyi Z, Freund TF (1993) Postsynaptic targets of GABAergic hippocampal neurons in the medial septum-diagonal band of broca complex. *J Neurosci* 13: 3712-24.

Ulanovsky N, Moss CF (2007) Hippocampal cellular and network activity in freely moving echolocating bats. *Nat Neuroscience* 10:224-33.

Vanderwolf CH (1969) Hippocampal electrical activity and voluntary movement in the rat. *Electroencephalogr Clin Neurophysiol* 26: 407-18.

Vanderwolf CH (1971)Limbic-diencephalic mechanisms of voluntary movement. *Psychol Rev* 78: 83-113.

Vanderwolf CH, Bland BH (1975) Two types of hippocampal rhythmical slow activity in both the rabbit and the rat: relations to behavioral and effects of atropine, diethyl ether, urethane, and pentobarbital. *Exp Neurol* 49:58-85.

Vertes RP (1992) PHA-L analysis of projections from the supramammillary nucleus in the rat. *J Comp Neurol* 326: 595-622.

Vertes RP, Kocsis B (1997) Brainstem-diencephalo-septohippocampal systems controlling the theta rhythm of the hippocampus. *Neuroscience* 81:893-926.

Vertes RP, Fortin WJ, Crane AM (1999) Projections of the median raphe nucleus in the rat. *J Comp Neurol* 407:555-582.

Vinogradova OS (1995) Expression, control, and probable functional significance of the neuronal theta-rhythm. *Prog Neurobiol* 45:523-583.

Wainer BH, Levey AI, Rye DB, Mesulam MM, Mufson EJ (1985) Cholinergic and non-cholinergic septohippocampal pathways. *Neurosci Letters* 54:45-52.

Wiener Si, Berthoz A, Zugaro MB (2002) Multisensory processing in the elaboration of place and head direction responses by limbic system

neurons. *Cog Brain Res* 14:45-90.

Whishaw IQ (1972) Hippocampal electroencephalographic activity in the Mongolian gerbil during natural behaviours and wheel running and in the rat during wheel running and conditioned immobility. *Can J Psychol* 26: 219-39.

Whishaw IQ, Vanderwolf CH (1973) Hippocampal EEG and behavior: changes in amplitude and frequency of RSA (theta rhythm) associated with spontaneous and learned movement patterns in rats and cats. *Behav Biol* 8:461-84.

Whishaw IQ, Maaswinkel H (1998) Rats with fimbria-fornix lesions are impaired in path integration: a role for the hippocampus in “sense of direction”. *J Neurosci* 8:3050-3058.

Wilson MA, McNaughton BL (1993) Dynamics of the hippocampal ensemble code for space. *Science* 261: 1055-8.

Winson J (1978) Loss of hippocampal theta rhythm results in spatial memory deficit in the rat. *Science* 201:160-163.

Wouterlood FG, Saldana E, Witter MP (1990) Projections from the nucleus reuniens thalami to the hippocampal region: light and electron microscopic tracing study in the rat with the anterograde tracer *phaseolus vulgaris*-leucoagglutinin. *J Comp Neurol* 296:179-203.

Wyble BP, Hyman JM, Rossi CA, Hasselmo ME. (2004) Analysis of theta power in hippocampal EEG during bar pressing and running behavior in rats during distinct behavioral contexts. *Hippocampus* 14:662-74.

Ylinen A, Soltesz I, Bragin A, Penttonen M, Sik A, Buzsaki G (1995) Intracellular correlates of hippocampal theta rhythm in identified pyramidal cells, granule cells and basket cells. *Hippocampus* 5: 78-90.

Zhang H, Lin SC, Nicolelis MAL (2010) Spatiotemporal coupling between hippocampal acetylcholine release and theta oscillations in vivo. *J Neurosci* 30:13431:13440.